September 1989

UILU-ENG-89-2227
DC-114

(2)

COORDINATED SCIENCE LABORATORY
College of Engineering
Decision and Control Laboratory

ARC CURRENT CONTROL OF A ROBOTIC WELDING SYSTEM: MODELING AND CONTROL SYSTEM DESIGN

Bruce William Greene

UNIVERSITY OF ILLINOIS AT URBANA-CHAMPAIGN

UNCLASSIFIED

SECURITY CLASSIFICATION OF THIS PAGE

REPORT DOCUMENTATION PAGE

1a. REPORT SECURITY CLASSIFICATION Unclassified	1b. RESTRICTIVE MARKINGS
2a. SECURITY CLASSIFICATION AUTHORITY	3. DISTRIBUTION / AVAILABILITY OF REPORT Approved for public release; distribution unlimited.
2b. DECLASSIFICATION / DOWNGRADING SCHEDULE	
4. PERFORMING ORGANIZATION REPORT NUMBER(S) UILU-ENG-89-2227 DC-114	5. MONITORING ORGANIZATION REPORT NUMBER(S)
6a. NAME OF PERFORMING ORGANIZATION Coordinated Science Lab University of Illinois 6b. OFFICE SYMBOL (If applicable) N/A	7a. NAME OF MONITORING ORGANIZATION U. S. Army Research Office
6c. ADDRESS (City, State, and ZIP Code) 1101 W. Springfield Avenue Urbana, IL 61801	7b. ADDRESS (City, State, and ZIP Code) P. O. Box 12211 Research Triangle Park, NC 27709-2211
8a. NAME OF FUNDING / SPONSORING ORGANIZATION U. S. Army Research Office 8b. OFFICE SYMBOL (If applicable)	9. PROCUREMENT INSTRUMENT IDENTIFICATION NUMBER DACA 88-88-M-1554
8c. ADDRESS (City, State, and ZIP Code) P. O. Box 12211 Research Triangle Park, NC 27709-2211	10. SOURCE OF FUNDING NUMBERS PROGRAM ELEMENT NO. / PROJECT NO. / TASK NO. / WORK UNIT ACCESSION NO.

11. TITLE (Include Security Classification)

ARC CURRENT CONTROL OF A ROBOTIC WELDING SYSTEM: MODELING AND CONTROL SYSTEM DESIGN

12. PERSONAL AUTHOR(S)
GREENE, BRUCE WILLIAM

13a. TYPE OF REPORT	13b. TIME COVERED	14. DATE OF REPORT (Year, Month, Day)	15. PAGE COUNT
Technical	FROM _____ TO _____	1989 September	51

16. SUPPLEMENTARY NOTATION The view, opinions and/or findings contained in this report are those of the author(s) and should not be construed as an official Department of the Army position, policy, or decision, unless so designated by other documentation.

17. COSATI CODES			18. SUBJECT TERMS (Continue on reverse if necessary and identify by block number)
FIELD	GROUP	SUB-GROUP	Wire feed plant; linear dynamics, severe torque disturbance; nonlinear arc dynamics

19. ABSTRACT (Continue on reverse if necessary and identify by block number)

This research was conducted as part of a joint project for the University of Illinois and the Metallurgy and Quality Assurance Team of the United States Army's Construction Engineering Research Laboratory. The ultimate objective of the program is to develop an automated welding system that produces consistently good welds despite variations in material parameters and other disturbances. The scope of the research is limited to consumable-electrode gas metal arc welding (GMAW) since this is one of the most frequently employed and economically important welding processes. Arc current is one of the key process variables that must be controlled if weld quality is to be maintained. This aspect of weld quality control is the focus of this report.

20. DISTRIBUTION / AVAILABILITY OF ABSTRACT ☐ UNCLASSIFIED/UNLIMITED ☐ SAME AS RPT. ☐ DTIC USERS	21. ABSTRACT SECURITY CLASSIFICATION Unclassified
22a. NAME OF RESPONSIBLE INDIVIDUAL	22b. TELEPHONE (Include Area Code) / 22c. OFFICE SYMBOL

DD FORM 1473, 84 MAR 83 APR edition may be used until exhausted. All other editions are obsolete.

SECURITY CLASSIFICATION OF THIS PAGE
UNCLASSIFIED

ARC CURRENT CONTROL OF A ROBOTIC WELDING SYSTEM: MODELING AND CONTROL SYSTEM DESIGN

BY

BRUCE WILLIAM GREENE

B.S., University of Illinois, 1988

THESIS

Submitted in partial fulfillment of the requirements
for the degree of Master of Science in Electrical Engineering
in the Graduate College of the
University of Illinois at Urbana-Champaign, 1989

Urbana, Illinois

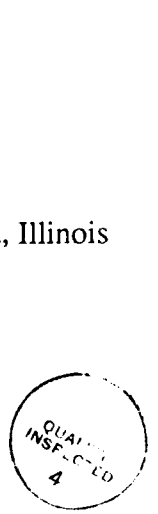

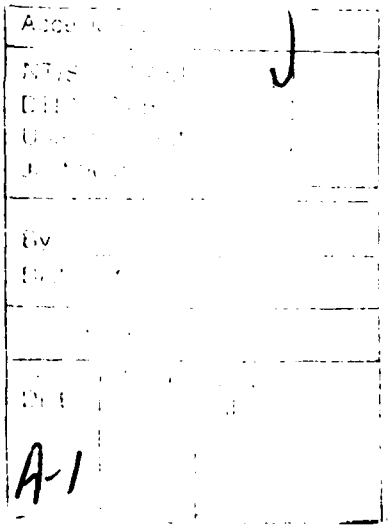

ACKNOWLEDGMENTS

I would like to sincerely thank my advisor, Professor P. V. Kokotovic, for his guidance and motivation and for his example of uncompromising dedication to the field of engineering.

I want to give special thanks to Ph.D. candidate Jeffrey Louis Schiano, whose day-to-day guidance is in no small part responsible for the quality of this work. If Professor Kokotovic were my father, then Jeff would surely have been my wise older brother.

Many thanks are also due to Frank Kearney of the United States Army Construction Engineering Research Laboratory for his support and for the excellent research environment that he provided.

I am most appreciative for the assistance in thesis preparation given to me by my good friend Kevin Buescher.

Finally, I would like to express my gratitude to my Mother, whose love and unending support were always given freely in times of need.

TABLE OF CONTENTS

CHAPTER 1.

INTRODUCTION

The following research was conducted as part of a joint project for the University of Illinois and the Metallurgy and Quality Assurance Team of the United States Army's Construction Engineering Research Laboratory. The ultimate objective of the program is to develop an automated welding system which produces consistently good welds despite variations in material parameters and other disturbances. The scope of the research is limited to consumable-electrode gas metal arc welding (GMAW) since this is one of the most frequently employed and economically important welding processes.

It is well known that the reliability of the weld is strongly correlated to the microstructure and gross geometry of the joint. These properties are determined by the thermal and mechanical history of the weld puddle and the rate at which it cools. The thermomechanical dynamics are driven by the flow of heat and mass from the torch as it travels along the weld joint. Arc current is one of the key process variables that must be controlled if weld quality is to be maintained. This aspect of weld quality control is the focus of this work.

A gearmotor drives a set of pinch rollers which feed wire down through the torch head for consumption in the welding process. The arc current is determined by the rate of wire feed. Arc current control is accomplished through a two-step design. First, a closed-loop wire feed servo is developed which can track a reference wire feed rate. Second, an arc current controller is designed which provides the reference for the wire feed servo.

Chapter 2 develops the wire feed mechanism model for use in the wire feed servo controller design of Chapter 3. Chapter 4 derives the arc dynamics model which relates arc current to wire feed rate. Chapter 5 makes use of this model along with the wire feed servo dynamics for the closed-loop arc current controller design. The Appendix provides plots derived from computer simulation as well as from experimental data to support the viability of the design.

CHAPTER 2.

WIRE FEED MECHANISM MODEL

2.1. Overview of the Wire Feed System

The electro-mechanical wire feed system shown in Figure 2.1 forms the *plant* around which the closed-loop wire feed servo is designed. The input of this plant is taken to be a discrete-time signal u(k) which is zero-order-held and power-amplified to drive a dc motor. The motor, in turn, drives a set of pinch rollers through a reduction gearbox. The discrete-time output $e_T(k)$ is defined to be the sampled voltage of a tachometer on the motor. This signal, properly scaled, yields a sampling of the wire feed rate $w_F(t)$ in inches-per-minute.

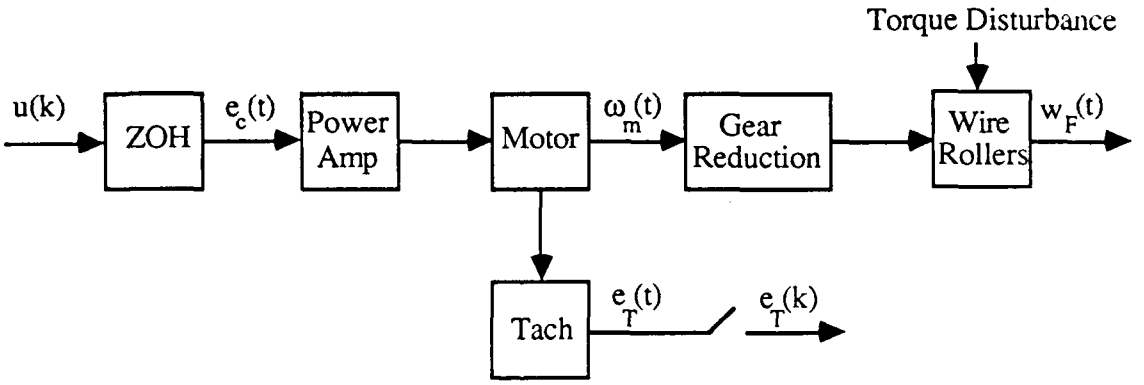

Figure 2.1. Wire feed mechanism block diagram.

The zero-order-hold (ZOH) digital to analog converter has an integer input $u(k) \in \{-2048, \ldots, 2048\}$ and a real output $e_c(t) \in [-5, 5]$ volts. The power amplifier is modeled as a fixed x4 gain block. This simplification of the power amplifier dynamics is valid because the dominant time constant of the motor is two orders of magnitude larger that that of the amplifier. A detailed analysis of the dc motor dynamics will be presented in Section 2.2. The system employs a 65.5:1 gearmotor with a torque efficiency of 66%. The tachometer conversion constant is 2 volts per 1000 rpm. Noiseless tach measurements are assumed. The pinch rollers have a diameter of

1.626 inches. A torque disturbance is introduced due to eccentricities in the wire roller mechanism and due to the friction of the wire feed path as shown in Figure 2.2.

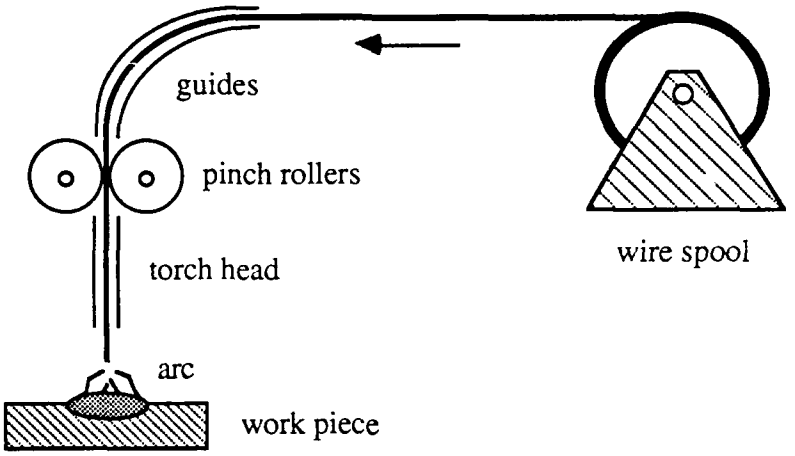

Figure 2.2. Wire path.

2.2. Direct Current Motor Model

The dc motor of Figure 2.3 is modeled as a series connection of equivalent armature resistance and inductance, and an ideal motor (Kuo (1980)).

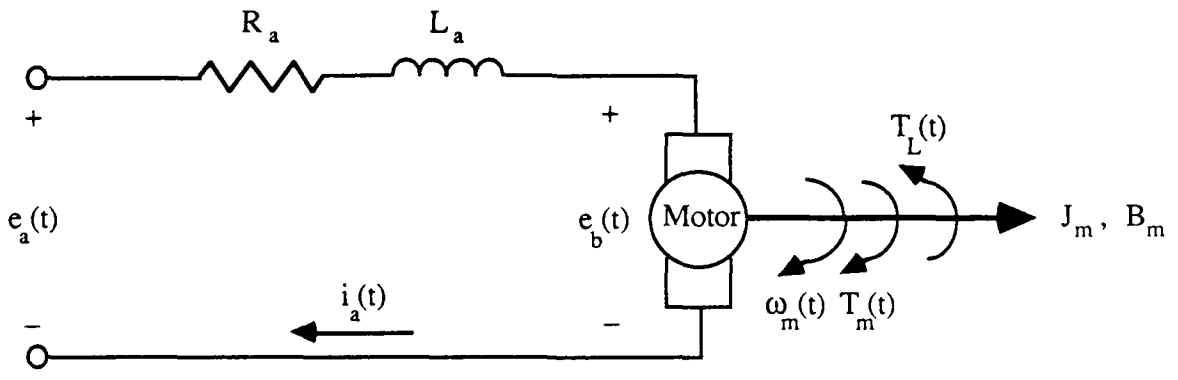

Figure 2.3. Direct current motor model.

Signals and Constants:

$e_a(t)$	armature voltage	R_a	armature resistance
$i_a(t)$	armature current	L_a	armature inductance
$e_b(t)$	back emf voltage	K_b	back emf constant
$\omega_m(t)$	shaft velocity	J_m	rotor inertia
$T_m(t)$	torque developed by motor	K_i	torque constant
$T_L(t)$	load torque	B_m	viscous frictional coefficient

The dc motor's dynamic equations are now developed. Kirchoff's Voltage Law around the armature loop yields the electrical constraint equation

$$e_a(t) = R_a\, i_a(t) + L_a \frac{di_a(t)}{dt} + e_b(t)\,. \tag{2.1}$$

Newton's Second Law gives the mechanical constraint equation

$$T_m(t) = T_L(t) + B_m\, \omega_m(t) + J_m \frac{d\omega_m(t)}{dt}. \tag{2.2}$$

The electro-mechanical coupling equations are

$$T_m(t) = K_i\, i_a(t)\,, \quad \text{and} \quad e_b(t) = K_b\, \omega_m(t)\,. \tag{2.3}$$

The state equations for the motor dynamics are now obtained by substituting equations (2.3) into (2.1) and (2.2).

$$\frac{di_a(t)}{dt} = -\frac{R_a}{L_a}\, i_a(t) - \frac{K_b}{L_a}\, \omega_m(t) + \frac{1}{L_a} e_a(t)\,, \tag{2.4}$$

$$\frac{d\omega_m(t)}{dt} = -\frac{B_m}{J_m}\, \omega_m(t) + \frac{K_i}{J_m} i_a(t) - \frac{1}{J_m} T_L(t)\,, \tag{2.5}$$

where the motor constants

$R_a = 2.55 \times 10^{1}\ \Omega$ $\qquad$ $K_b = 2.31 \times 10^{-2}\ \frac{V \cdot s}{rad}$ $\qquad$ $K_i = 3.27 \times 10^{1}\ \frac{oz \cdot in}{A}$

$L_a = 2.04 \times 10^{-3}\ H$ $\qquad$ $J_m = 5.37 \times 10^{-4}\ oz \cdot in \cdot s^2$ $\qquad$ $B_m = 1.00 \times 10^{-3}\ \frac{oz \cdot in \cdot s}{rad}$

are obtained from the manufacturer's specification sheets.

Analysis of the system time constants reveals a valid simplification. Make the following two definitions:

$$\text{Electrical time constant} \qquad \tau_e := \frac{L_a}{R_a} = 8.00 \times 10^{-4}\ \text{s},$$

$$\text{Mechanical time constant} \qquad \tau_m := \frac{J_m}{B_m} = 5.37 \times 10^{-1}\ \text{s}.$$

Time constant τ_m exceeds τ_e by more than two orders of magnitude. This suggests that it is reasonable to neglect the *electrical* dynamics. Consider (2.4) multiplied by the armature inductance L_a :

$$L_a \frac{di_a(t)}{dt} = - R_a i_a(t) - K_b \omega_m(t) + e_a(t) . \tag{2.6}$$

Since L_a is small, (2.6) may be approximated by

$$0 \approx - R_a i_a(t) - K_b \omega_m(t) + e_a(t) . \tag{2.7}$$

Solving (2.7) for the armature current $i_a(t)$ gives

$$i_a(t) \approx \frac{e_a(t) - K_b \omega_m(t)}{R_a} . \tag{2.8}$$

Substitution of (2.8) into (2.5) yields a *first-order* model of the motor dynamics:

$$\frac{d\omega_m}{dt} = - p_m \omega_m(t) + \frac{1}{J_m} u_T(t) , \tag{2.9}$$

where

$$p_m := \frac{B_m}{J_m} + \frac{K_i K_b}{J_m R_a} , \tag{2.10}$$

and

$$u_T(t) := \frac{K_i}{R_a} e_a(t) - T_L(t) . \tag{2.11}$$

Taking the Laplace transform of (2.9) gives

$$\frac{\Omega_m(s)}{U_T(s)} = \frac{1 / J_m}{s + p_m} .$$

The resulting transfer function description of the dc motor is shown in Figure 2.4.

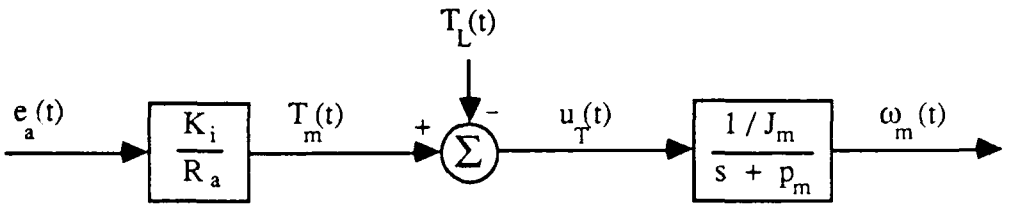

Figure 2.4. Direct current motor block diagram.

The manufacturer's specifications for the wire feed motor yield the following numerical values:

$$\frac{K_i}{R_a} = 1.28 \ \frac{oz{\cdot}in}{V}, \quad \frac{1}{J_m} = 1.86 \times 10^3 \ \frac{1}{oz{\cdot}in{\cdot}s^2}, \quad p_m = 57.025 \ \frac{rad}{s}.$$

Note that the wire feed motor acts as a *low-pass filter* with a cutoff frequency of 9.1 Hz.

2.3. Torque Disturbance Model

The wire feed gearmotor turns a set of spring-loaded pinch rollers which pull wire from a large spool, through a series of guides, and down to the torch head (See Figure 2.2). The resulting torque load on the motor has two principal components. There is a large constant load due to the stiffness of the wire and the friction of the guides, rollers, and bearings. In addition, mechanical imperfections in the pinch roller assembly cause an eccentricity that gives rise to an approximately sinusoidal term.

The total torque load on the gearmotor shaft is modeled as

$$T_G(t) = A + B \sin(2\pi f_D t). \tag{2.12}$$

This torque at the gearbox is a product of the torque load on the motor, the torque efficiency of the gearbox, and the gear reduction ratio. Reflect the gearbox torque back through the reduction gears to obtain the torque load on the motor shaft:

$$T_L(t) = (0.66)^{-1} (65.5)^{-1} T_G(t) = 0.0231 \ T_G(t). \tag{2.13}$$

The frequency of the sinusoidal component is proportional to the wire feed rate:

$$f_D = \frac{1}{\pi} \frac{1 \text{ revolution}}{1.626 \text{ in}} \frac{1 \text{ min}}{60 \text{ s}} w_F = 3.26 \times 10^{-3} w_F , \qquad (2.14)$$

where 1.626 inches is the diameter of each pinch roller and the wire feed rate w_F is given in inches per minute.

Equations (2.12) and (2.14) reflect a key *assumption*. Wire feed rate w_F is taken to be *constant* in (2.14), resulting in a constant disturbance frequency f_D in (2.12). However, w_F actually fluctuates in response to computer commands during control of the weld process. This complication, along with the fact that $T_L(t)$ can also affect w_F through the motor dynamics, cause the disturbance to be not truly sinusoidal. The frequency f_D actually approximates only the principal component of the disturbance. The simplification is validated by the fact that this principal component is the only one that has a severe effect on the wire feed rate. Figure A.2 of the Appendix shows a typical wire feed rate signal taken from experimental open-loop data. A Fourier transform of the signal shows that a principal component is indeed present at near the predicted frequency.

Extensive open-loop experiments show that typical values for constants A and B in (2.12) are 141 and 15.0 oz·in respectively. Reasonable wire feed rates lie in the 200-400 IPM range, resulting in disturbance frequencies of 0.65-1.3 Hz. These facts yield a typical torque load at the motor shaft of

$$T_L(t) \approx 3.27 + 0.35 \sin(2\pi f_D t) \text{ oz·in}, \quad 0.65 \text{ Hz} \leq f_D \leq 1.3 \text{ Hz} . \qquad (2.15)$$

Section 2.2 shows that the wire feed motor responds to frequencies exceeding 9 Hz. Since wire feed rate is a principal variable in the control of weld quality, a successful wire feed servo controller must attenuate this disturbance as much as possible.

2.4. Discretization of the Wire Feed Mechanism Model

Since wire feed rate control is to be accomplished with a digital computer, a discrete-time model of the wire feed mechanism is necessary. Insertion of the first-order motor model of Figure 2.4 into the wire feed mechanism block diagram of Figure 2.1 yields Figure 2.5.

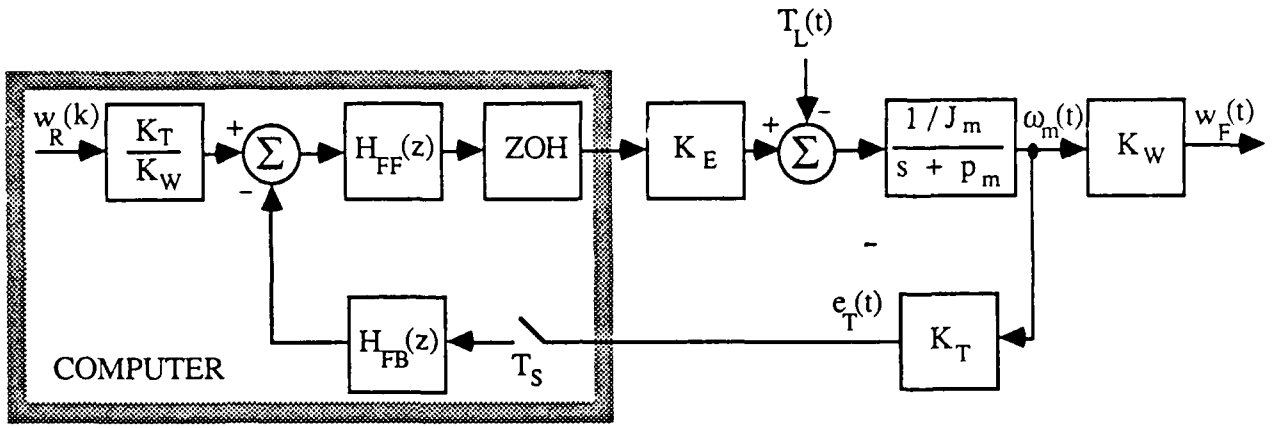

Figure 2.5. Wire feed servo block diagram.

The reference wire feed rate $w_R(k)$ is given in inches per minute. Figure 2.5 provides for a *two degree of freedom* controller structure that features both feedforward and feadback filters.

The scaling factor K_W converts motor angular velocity ω_m (rad·s^{-2}) into wire feed rate w_F (IPM). Figures 2.1 and 2.2 yield

$$K_W = \frac{1}{65.5} \frac{\pi \cdot 1.626 \text{ in}}{1 \text{ revolution}} \frac{1 \text{ revolution}}{2\pi \text{ rad}} \frac{60 \text{ s}}{1 \text{ min}} = 0.7447 \frac{\text{IPM} \cdot \text{s}}{\text{rad}} .$$

The factor K_T converts motor angular velocity ω_m into the tachometer voltage e_T.

$$K_T = \frac{1}{5} \frac{2 \text{ V}}{1000 \text{ RPM}} \frac{1 \text{ revolution}}{2\pi \text{ rad}} \frac{60 \text{ s}}{1 \text{ min}} = 3.820 \times 10^{-3} \frac{\text{V} \cdot \text{s}}{\text{rad}} .$$

Finally, K_E converts the computer control voltage u into torque (oz·in).

$$K_E = \frac{4 K_i}{R_a} = 5.129 \frac{\text{oz} \cdot \text{in}}{\text{V}} .$$

Discretization of the continuous-time dc motor transfer function is accomplished through the use of the hold equivalence method (Franklin & Powell (1980)):

$$G(z) = (1 - z^{-1})\, \mathcal{Z}\left\{ \frac{1/J_m}{s\,(s + p_m)} \right\} .$$

The Z-transform may be evaluated by using the transform pair

$$\mathcal{Z}\left\{ \frac{a}{s\,(s + a)} \right\} \longleftrightarrow \frac{z\,(1 - e^{-aT})}{(z - 1)(z - e^{-aT})} \quad ; \qquad T := \text{sample period} .$$

This yields

$$G(z) = \frac{1}{J_m\, p_m} \frac{1 - \exp(-p_m T_S)}{z - \exp(-p_m T_S)} . \tag{2.16}$$

Make the following definition:

$$G(z) := \frac{K_D}{z - p_D} , \tag{2.17}$$

where

$$K_D = \frac{1}{J_m\, p_m} [\, 1 - \exp(-p_m T_S)\,] ,$$

and

$$p_D = \exp(-p_m T_S) .$$

A discrete-time model of the entire wire feed servo system is shown in Figure 2.6.

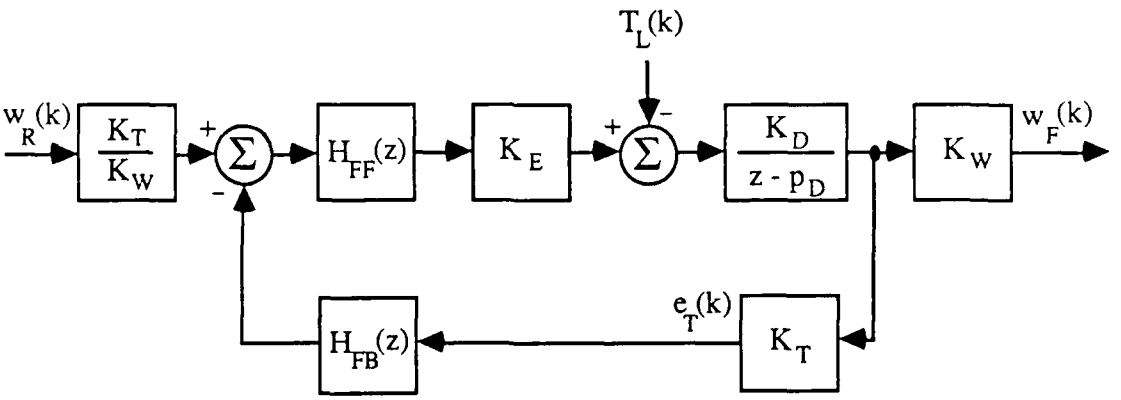

Figure 2.6. Discretized wire feed servo block diagram.

Analysis and controller design are simplified by introducing the *normalized* model of Figure 2.7.

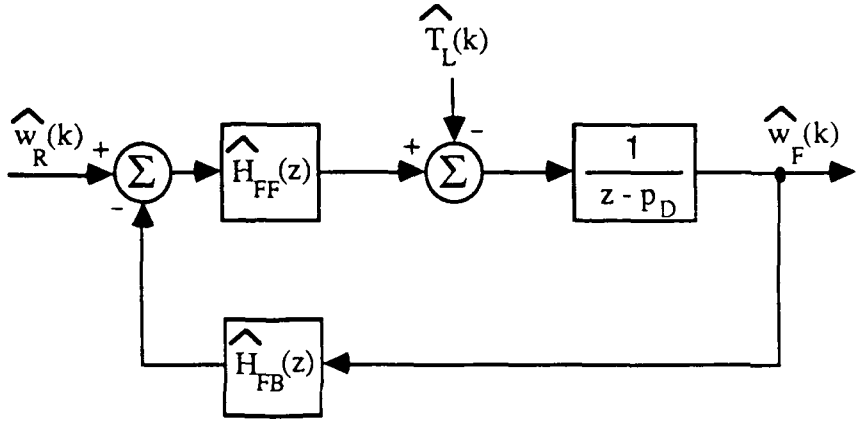

Figure 2.7. Discretized and normalized wire feed servo block diagram.

where

$$\hat{w}_R(k) = \frac{K_T}{K_W} w_R(k) , \qquad \hat{H}_{FF}(z) = K_E K_D K_T H_{FF}(z) ,$$

$$\hat{w}_F(k) = \frac{K_T}{K_W} w_F(k) , \qquad \hat{H}_{FB}(z) = H_{FB}(z) ,$$

$$\hat{T}_L(k) = K_D K_T T_L(k) .$$

The controller design is carried out on the normalized system for simplicity. Then the actual controller filters $H_{FF}(z)$ and $H_{FB}(z)$ are found from the normalized ones.

CHAPTER 3.

WIRE FEED SERVO CONTROLLER DESIGN

3.1. Design Objectives

The wire feed servo is a closed-loop system within the arc current control loop as shown in Figure 3.1. It is important to consider the system as a whole while formulating the design objectives for each subsystem. This nested control-loop structure allows the two controllers to share the burden of the total design.

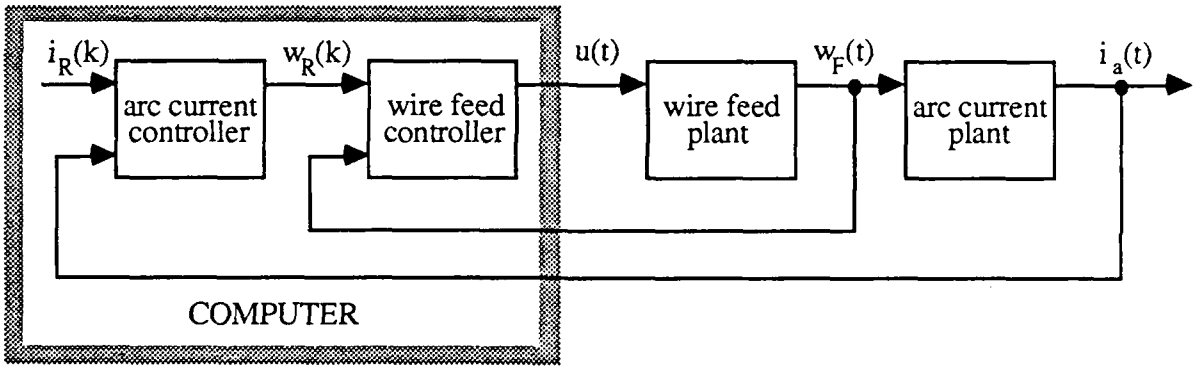

Figure 3.1. Nested control-loop structure.

The wire feed servo must, of course, exhibit zero steady-state error for a constant reference signal $w_R(k)$. In addition, the wire feed plant is subjected to a disturbance torque of the form

$$T_L(t) \approx A + B \sin(2\pi f_D t) \text{ oz·in}, \quad 0.65 \text{ Hz} \leq f_D \leq 1.3 \text{ Hz}. \tag{3.1}$$

This disturbance must be attenuated as much as possible since it falls within the passband of the arc dynamics.

High frequency arc noise occurs which should be attenuated around the loop so that it does not interfere with tracking of the reference signal $i_R(k)$. For this reason the wire feed servo's bandwidth will be limited to 4.0 Hz. A damping ratio ζ of 0.707 will yield a reasonable step response.

Chapter 1 ended with the development of the discretized and normalized wire feed servo block diagram of Figure 3.2.

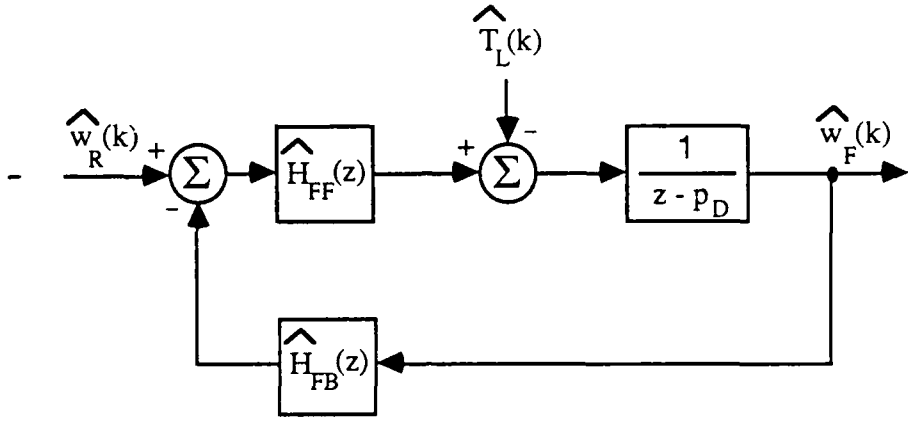

Figure 3.2. Discretized and normalized wire feed servo block diagram.

The controller transfer functions $\hat{H}_{FF}(z)$ and $\hat{H}_{FB}(z)$ must be designed to accomplish the objectives stated above.

The sampling interval T_S is selected according to a practical rule given in Astrom & Wittenmark (1984). *The sampling rate should be six to ten times the closed-loop bandwidth.*

$$4 \text{ Hz BW} \quad \Rightarrow \quad 24 \text{ Hz} \le \frac{1}{T_S} \le 40 \text{ Hz} \quad \Rightarrow \quad 0.025 \text{ s} \le T_S \le 0.042 \text{ s}. \qquad (3.2)$$

A sampling interval T_S of 0.04 second will be used for data conversion.

Numerical values for the discretized plant parameters K_D and p_D may now be calculated:

$$K_D = \frac{1}{J_m p_m}[\, 1 - \exp(-p_m T_S)\,] = 29.3159,$$

and

$$p_D = \exp(-p_m T_S) = 0.102182.$$

The design objectives relating to reference tracking characteristics may be conveniently met by selecting a desired reference-to-output transfer function. Consider the continuous-time, second-order transfer function

$$H_{cl}(s) := \frac{\hat{W}_F(s)}{\hat{W}_R(s)} = \frac{\omega_n^2}{s^2 + 2\zeta\omega_n s + \omega_n^2} . \tag{3.3}$$

$H(j\omega)$ has $\log_{10}$ magnitude given by

$$\left| H_{cl}(j\omega) \right|_{dB} = -20 \log_{10} \sqrt{\left(1 - \frac{\omega^2}{\omega_n^2} \right)^2 + \left(\frac{2\zeta\omega}{\omega_n} \right)^2} . \tag{3.4}$$

The zero steady-state tracking error requirement is achieved because $\left| H_{cl}(0) \right|_{dB}$ is zero for any choice of ζ and ω_n. The damping ratio ζ can be specified directly and the natural frequency ω_n can be chosen to obtain a 4 Hz bandwidth. Define ω_c to be the cutoff frequency. We must have

$$\omega_c = 2\pi f_c = 2\pi (4 \text{ Hz}) = 8\pi \text{ rad} \cdot \text{s}^{-1} , \tag{3.5}$$

$$-3 \text{ dB} = \left| H_{cl}(j\omega_c) \right|_{dB} = -20 \log_{10} \sqrt{\left(1 - \frac{\omega_c^2}{\omega_n^2} \right)^2 + \left(\frac{2\zeta\omega_c}{\omega_n} \right)^2} . \tag{3.6}$$

Simplification of (3.6) yields

$$2 = \left(1 - \frac{\omega_c^2}{\omega_n^2} \right)^2 + \left(\frac{2\zeta\omega_c}{\omega_n} \right)^2 . \tag{3.7}$$

Substitution of the desired ζ of $\sqrt{\frac{1}{2}}$ results in

$$\omega_n = \omega_c . \tag{3.8}$$

Thus the natural frequency is equal to the cutoff frequency for this choice of damping ratio.

The desired continuous-time transfer function is now given by

$$H_{cl}(s) = \frac{631.655}{s^2 + 35.5431s + 631.655} . \tag{3.9}$$

The *zero-order-hold equivalent* discretization of H(s) is found with the aid of Table 3.1 of Astrom & Wittenmark (1984).

$$H_{cl}(z) := \frac{\hat{W}_F(z)}{\hat{W}_R(z)} = \frac{b_1 z + b_2}{z^2 + a_1 z + a_2} . \tag{3.10}$$

The coefficients b_1, b_2, a_1, and a_2 are found as follows:

$$\omega = \omega_n\sqrt{1 - \zeta^2} = 17.7715 , \qquad b_1 = 1 - \alpha\left(\frac{\zeta\omega_n}{\omega}\gamma + \beta\right) = 0.307238 ,$$

$$\alpha = \exp(-\zeta\omega_n T_S) = 0.491221 , \qquad b_2 = \alpha^2 + \alpha\left(\frac{\zeta\omega_n}{\omega}\gamma - \beta\right) = 0.189566 ,$$

$$\beta = \cos(\omega T_S) = 0.757800 , \qquad a_1 = -2\alpha\beta = -0.744495 ,$$

$$\gamma = \sin(\omega T_S) = 0.652487 , \qquad a_2 = \alpha^2 = 0.241298 .$$

Substitution of these numerical values into (3.10) yields

$$H_{cl}(z) := \frac{\hat{W}_F(z)}{\hat{W}_R(z)} = \frac{0.307238\, z + 0.189566}{z^2 - 0.744495\, z + 0.241298} . \tag{3.11}$$

The objectives for the wire feed servo controller design are now reduced to the attenuation of the torque disturbance and the achievement of the desired reference-to-output transfer function of (3.11). Figure A.1 of the Appendix shows magnitude plots of the open-loop wirefeed plant (plot 1) and the desired reference-to-output transfer function (plot 2).

3.2. Proportional-Sum Controller Design

A simple proportional-plus-sum digital control strategy is employed to achieve the design objectives as closely as possible.

$$\hat{H}_{FF}(z) = K_P + \frac{K_S}{z - 1} = \frac{K_P z + (K_S - K_P)}{z - 1}, \qquad \hat{H}_{FB}(z) = 1. \tag{3.12}$$

Insertion of this controller into the block diagram of Figure 3.2 yields Figure 3.3.

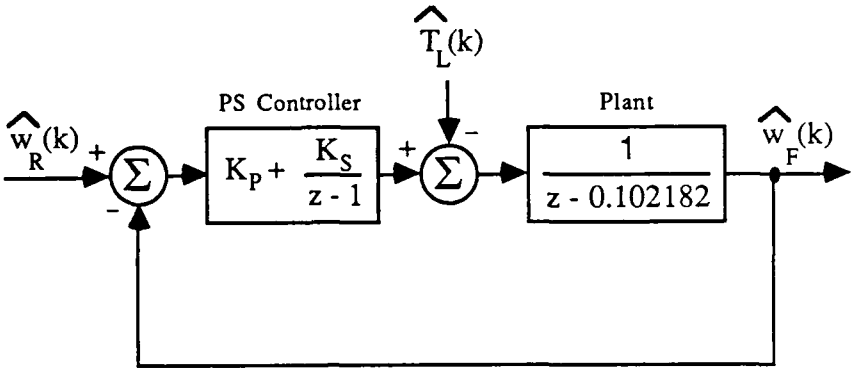

Figure 3.3. PS controlled wire feed servo block diagram.

The accumulator action in the feed-forward controller gives zero steady-state tracking error for constant reference inputs as well as rejection of constant disturbances. However, since only the two design parameters K_P and K_S exist, an exact matching of the desired reference-to-output transfer function of (3.11) is impossible. The desired characteristic equation can be obtained but then no degrees of freedom will remain with which to place the closed-loop zero.

The reference-to-output transfer function is given by

$$H_{cl}(z) = \frac{\hat{W}_F(z)}{\hat{W}_R(z)} = \frac{K_P z + (K_S - K_P)}{(z - 0.102182)(z - 1) + K_P z + (K_S - K_P)}. \tag{3.13}$$

Define the characteristic equation (denominator of the closed-loop transfer function) to be $\Delta(z)$.

$$\Delta(z) = z^2 + (K_P - 1.102182)\, z + (K_S - K_P + 0.102182). \tag{3.14}$$

The desired characteristic equation of (3.11) is

$$\Delta(z) = z^2 - 0.744495\, z + 0.241298\,. \tag{3.15}$$

By setting (3.14) equal to (3.15) and equating coefficients of like powers of z, one obtains

$$\begin{aligned} K_P &= -0.744495 + 1.102182 = 0.357687 \\ K_S &= 0.241298 - 0.102182 + K_P = 0.496803\,. \end{aligned} \tag{3.16}$$

The resulting proportional-sum wirefeed controller is

$$\hat{H}_{FF}(z) = \frac{0.357687\, z + 0.139116}{z - 1} \tag{3.17}$$

$$\hat{H}_{FB}(z) = 1.$$

Plot 3 of Figure A.1 in the Appendix shows the magnitude of the closed-loop disturbance-to-output transfer function resulting from use of the PS controller of (3.17). The upper half of Figure A.3 shows a wirefeed experiment utilizing this controller. Comparison with Figure A.2 shows a reasonable amount of low frequency disturbance attenuation over the open-loop experimental results.

3.3. Polynomial Controller Design

The proportional-sum controller's simple structure does not utilize the feedback filter and this method only gives the designer two parameters to tune. In order to better accomplish the design objectives, the more sophisticated controller of Figure 3.4 will be used.

The design methodology presented in this section treats the various transfer functions as rational polynomials in z. This *polynomial method* provides a step-by-step way to construct a higher-order controller. See Chapter 10 of Astrom & Wittenmark (1984). This design will exactly match the desired reference-to-output transfer function. It will also improve low frequency disturbance rejection by placing a 1 Hz zero in the disturbance-to-output transfer function.

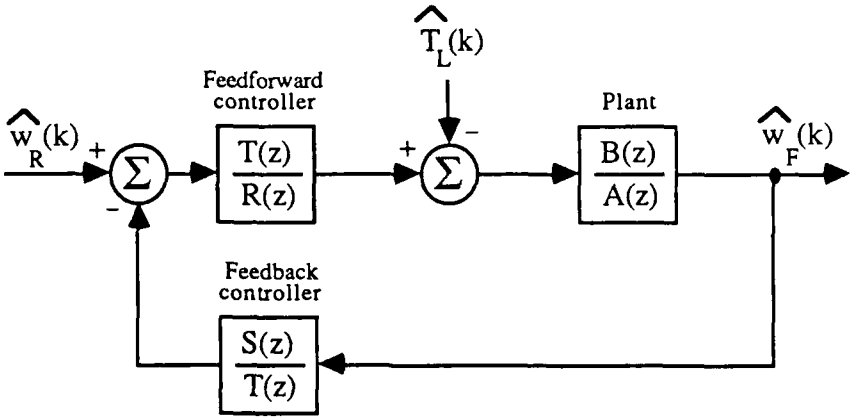

Figure 3.4. Polynomial representation of wire feed servo.

Throughout this section, H(z) will represent a *rational transfer function* in z, while all other capital letters will represent *polynomials* in z. A polynomial in z is of the form

$$P(z) = a_n z^n + a_{n-1} z^{n-1} + \ldots + a_1 z + a_0 \ ,$$

where the *degree* of P(z) is n, and P(z) is said to be *monic* if a_n is unity. With this notation in mind, the following definitions are presented:

$$\text{Plant:} \qquad H(z) := \frac{B(z)}{A(z)} = \frac{1}{z - 0.102182} \ , \tag{3.18}$$

$$\text{Model:} \qquad H_m(z) := \frac{B_m(z)}{A_m(z)} = \frac{0.307238\, z + 0.189566}{z^2 - 0.744495\, z + 0.241298} \ , \tag{3.19}$$

$$\text{Controller:} \qquad \hat{H}_{FF}(z) := \frac{T(z)}{R(z)} \ , \qquad \hat{H}_{FB}(z) := \frac{S(z)}{T(z)} \ . \tag{3.20}$$

The rational transfer functions of the controller must at least be proper in order for the controller to be causal and, therefore, implementable. Thus the polynomials R, S, and T must be such that

$$\deg(R) \geq \deg(T) \geq \deg(S) \ . \tag{3.21}$$

Furthermore, restrict polynomials A, A_m, and R to be monic and assume no pole-zero cancellation in either of the transfer functions H or H_m.

The plant and model polynomials can now be identified:

$$A(z) = z - 0.102182, \qquad B(z) = 1. \tag{3.22}$$

$$A_m(z) = z^2 - 0.744495\,z + 0.241298, \qquad B_m(z) = 0.307238\,z + 0.189566. \tag{3.23}$$

Examination of Figure 3.4 yields the following transfer functions:

$$\frac{\hat{W}_F(z)}{\hat{W}_R(z)} = \frac{\hat{H}_{FF}H}{1 + \hat{H}_{FF}\hat{H}_{FB}H}, \qquad \frac{\hat{W}_F(z)}{\hat{T}_L(z)} = \frac{H}{1 + \hat{H}_{FF}\hat{H}_{FB}H}. \tag{3.24}$$

Substitution of (3.18) and (3.20) into (3.24) gives

$$\frac{\hat{W}_F(z)}{\hat{W}_R(z)} = \frac{BT}{AR + BS}, \qquad \frac{\hat{W}_F(z)}{\hat{T}_L(z)} = \frac{BR}{AR + BS}. \tag{3.25}$$

Zero steady-state response to constant disturbances as well as to 1 Hz disturbances is required. The disturbance-to-output transfer function of (3.25) must have zeros at these frequencies. A polynomial of the form

$$P(z) = (z - r\,e^{j\theta})(z - r\,e^{-j\theta}) = z^2 - 2r\cos\theta\, z + r^2 \tag{3.26}$$

has complex conjugate zeros at

$$z = r\exp(\pm j\theta).$$

With the radius r set to one, P(z) has its zeros on the unit circle at angles $\pm\theta$. Thus P(z) will zero a sinusoid of frequency θ. A 1 Hz disturbance has a discrete-time normalized frequency given by

$$\theta = 2\pi f_D T_S = 2\pi(1\text{ Hz})(.04\text{ s}) = 0.2513\text{ rad.} \tag{3.27}$$

Consider a controller polynomial R(z) of the form

$$R(z) = (z - 1)[z^2 - 2\cos(0.2513)\,z + 1]. \tag{3.28}$$

From (3.25) it can be seen that a zero of R(z) will also be a zero of the disturbance-to-output transfer function. The (z - 1) term provides a zero at dc, while the quadratic term provides zeros at 1 Hz.

The reference-to-output transfer function is required to be $H_m(z)$. A comparison of (3.19) with (3.25) yields the restriction

$$\frac{BT}{AR + BS} = \frac{B_m}{A_m} . \tag{3.29}$$

Since R(z) has been specified as (3.28) and since A, B, A_m, and B_m are also fixed, only S and T remain free to satisfy (3.29). Recalling that B is unity for the normalized plant, it may be eliminated in order to write

$$T(z) = B_m(z) = 0.307238\, z + 0.189566 . \tag{3.30}$$

$$\begin{aligned} S(z) &= A_m(z) - A(z)R(z) \\ &= (z^2 - 0.744495\, z + 0.241298) - (z - 0.102182)(z - 1)(z^2 - 1.93718\, z + 1) . \end{aligned} \tag{3.31}$$

Unfortunately, this solution results in a noncausal controller since restriction (3.21) is violated. Notice that the degrees of R, S, and T are three, four, and one, respectively. This problem is elegantly solved by the introduction of an *observer polynomial* $A_o(z)$. Requirement (3.29) is unaltered by the modification

$$\frac{BT}{AR + BS} = \frac{B_m A_o}{A_m A_o} , \tag{3.32}$$

for any polynomial A_o. However, we now have the relations

$$T(z) = B_m(z)A_o(z) = (0.307238\, z + 0.189566)\, A_o . \tag{3.33}$$

$$\begin{aligned} S(z) &= A_m(z)A_o(z) - A(z)R(z) \\ &= (z^2 - 0.744495\, z + 0.241298)\, A_o - (z - 0.102182)(z - 1)(z^2 - 1.93718\, z + 1) . \end{aligned} \tag{3.34}$$

Careful examination of (3.33) and (3.34) reveals that *any monic A_o of degree two* will yield

$$\deg(R) = \deg(S) = \deg(T) = 3 , \tag{3.35}$$

resulting in proper third-order feedforward and feedback controllers. The observer polynomial derives its name from the fact that it is cancelled out of the reference-to-output transfer function just as the dynamics of a state-space observer would be. It does, however, appear in the denominator of the closed-loop disturbance-to-output transfer function.

$$\frac{\hat{W}_F(z)}{\hat{W}_R(z)} = \frac{BT}{AR + BS} = \frac{B_m A_o}{A_m A_o} , \qquad \frac{\hat{W}_F(z)}{\hat{T}_L(z)} = \frac{BR}{AR + BS} = \frac{R}{A_m A_o} . \tag{3.36}$$

The poles of this quadratic can be used to further improve the disturbance rejection without modifying the reference tracking characteristics. Their location was chosen by an iterative process of simulation. It was found that a frequency of 1 Hz and a radius of 0.6 yield the most desirable transfer function. Equation (3.26) gives

$$A_o(z) = z^2 - 2(0.6)\cos(0.08\pi)\, z + (0.6)^2 = z^2 - 1.16230\, z + 0.36 . \tag{3.37}$$

Substitution of (3.37) into (3.33) and (3.34) completes the design.

$$\begin{aligned} R(z) &= 1.000000\, z^3 - 2.937166\, z^2 + 2.937166\, z - 1.000000 , \\ S(z) &= 1.132553\, z^3 - 1.770668\, z^2 + 0.751647\, z - 0.015315 , \\ T(z) &= 0.307238\, z^3 - 0.167536\, z^2 - 0.109727\, z + 0.068244 . \end{aligned} \tag{3.38}$$

The resulting polynomial method wirefeed controller design is given by

$$\hat{H}_{FF}(z) = \frac{0.307238\, z^3 - 0.167536\, z^2 - 0.109727\, z + 0.068244}{z^3 - 2.937166\, z^2 + 2.937166\, z - 1.000000} , \tag{3.39}$$

$$\hat{H}_{FB}(z) = \frac{3.686248\, z^3 - 5.763188\, z^2 + 2.446468\, z - 0.049847}{z^3 - 0.545299\, z^2 - 0.357140\, z + 0.222120} .$$

Plot 4 of Figure A.1 in the Appendix shows the magnitude of the disturbance-to-output transfer function for this wirefeed controller. The lower half of Figure A.3 shows the results of a wirefeed experiment using the controller of (3.39). A comparison of this design with the proportional-sum design of Section 3.2 shows that the polynomial controller improves low frequency disturbance rejection while worsening performance at higher frequencies. This result can be predicted by examining the frequency responses of Figure A.1.

3.4. Two Degree of Freedom Controller Design

By forcing a zero at 1 Hz, the design of Section 3.3 accentuates higher frequency components of the torque disturbance. A controller that is capable of rejecting the strong low frequency components without amplifying the higher frequency ones is very desirable. To this end, temporarily ignore the reference input $w_R(k)$ and treat the wire feed servo as the simple SISO regulator of Figure 3.5.

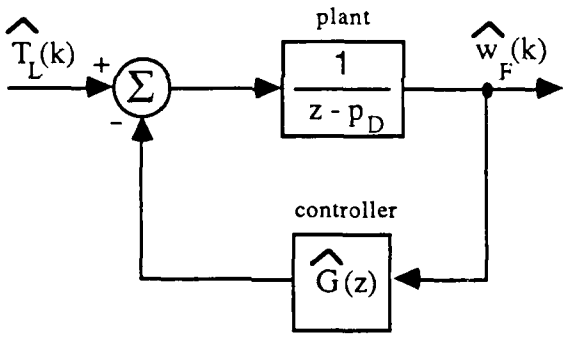

Figure 3.5. Wire feed regulator.

Let the controller $\hat{G}(z)$ have a simple proportional-sum structure.

$$\hat{G}(z) = K_P + \frac{K_S}{z - 1} = \frac{K_P z + (K_S - K_P)}{z - 1} . \qquad (3.40)$$

The accumulator action will guarantee zero steady-state error for constant torque disturbances just as it did in Section 3.2.

The closed-loop disturbance transfer function is given by

$$H_L(z) = \frac{\hat{W}_F(z)}{\hat{T}_L(z)} = \frac{z - 1}{(z - p_D)(z - 1) + K_P z + (K_S - K_P)} \tag{3.41}$$

$$= \frac{z - 1}{z^2 + (K_P - p_D - 1)z + (K_S - K_P + p_D)} .$$

The PS controller allows arbitrary placement of the closed-loop poles. The objective is to minimize the regulator's response to disturbance inputs all the way from dc out to the Nyquist frequency. The effect of pole location on the magnitude of the frequency response will now be considered with the aid of Figure 3.6.

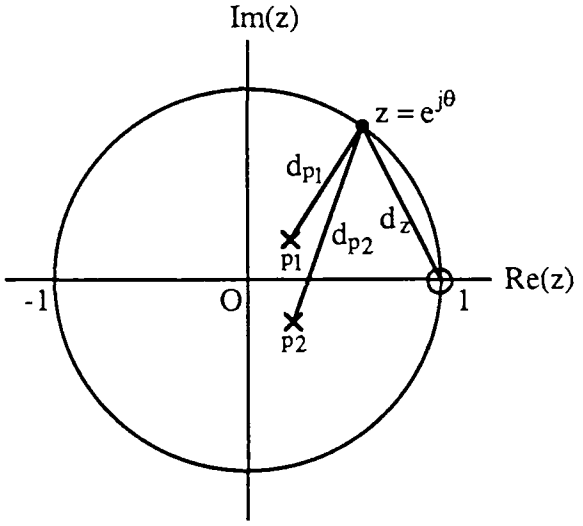

Figure 3.6. Z-plane pole-zero plot of $H_L(z)$.

Let d_i be the absolute distance from the ith pole or zero to the point on the unit circle that corresponds to the frequency of interest. Let the ith pole or zero be located at the point

$$z = x + jy .$$

This distance may be expressed as

$$d_i = \left| e^{j\theta} - x - jy \right| . \tag{3.42}$$

Now let the poles of $H_L(z)$ be located at $a \pm jb$. We have

$$H_L(z) = \frac{z - 1}{(z - a - jb)(z - a + jb)} , \tag{3.43}$$

and

$$\left| H_L(e^{j\theta}) \right| = \frac{\left| e^{j\theta} - 1 \right|}{\left| e^{j\theta} - a - jb \right| \left| e^{j\theta} - a + jb \right|} = \frac{d_z}{d_{P1}\, d_{P2}} . \tag{3.44}$$

Examination of (3.44) in conjunction with Figure 3.6 gives the designer considerable intuition. The zero at DC causes (3.44) to increase for higher frequencies. Extending this idea, we now see why an additional zero at 1 Hz causes the accentuation of high frequency disturbances. Conversely, the poles decrease (3.44) as they are placed farther away from the frequency of interest. Since the objective is to push the disturbance down as much as possible across the entire frequency range, it is readily seen that placing both poles at the origin is the best solution. A controller design that places all of the closed-loop poles at the origin is called a *deadbeat response* design (Kuo (1980)).

Thus we have a desired closed-loop disturbance-to-output transfer function:

$$H_L(z) = \frac{z - 1}{z^2} = \frac{z - 1}{z^2 + (K_P - p_D - 1)z + (K_S - K_P + p_D)} . \tag{3.45}$$

Matching coefficients of like powers of z in the denominators yields

$$K_P - p_D - 1 = 0 , \qquad K_S - K_P + p_D = 0 . \tag{3.46}$$

Recalling that p_D is 0.102182 and solving for the controller gains give

$$K_P = 1.1022 , \qquad K_S = 1.0000 , \tag{3.47}$$

and

$$\hat{G}(z) = \frac{K_P z + (K_S - K_P)}{z - 1} = \frac{1.1022z - 0.1022}{z - 1} . \tag{3.48}$$

Now that the desired torque disturbance controller $\hat{G}(z)$ has been designed, we can return to the full multi-input problem.

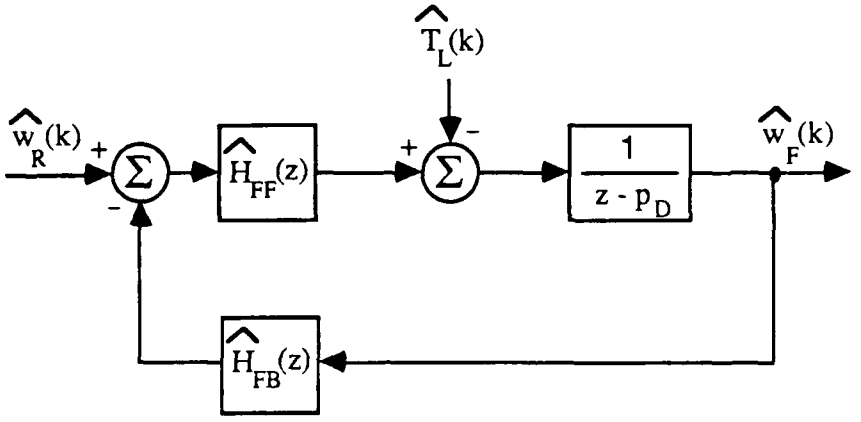

Figure 3.7. Full wire feed servo block diagram.

A comparison of Figures 3.5 and 3.7 results in the relation

$$\hat{G}(z) = \hat{H}_{FF}(z)\,\hat{H}_{FB}(z)\,. \tag{3.49}$$

Also from Figure 3.7,

$$H_R(z) := \frac{\hat{W}_F(z)}{\hat{W}_R(z)} = \frac{\hat{H}_{FF}H}{1 + \hat{H}_{FF}\hat{H}_{FB}H}\,, \tag{3.50}$$

and

$$H_L(z) := \frac{\hat{W}_F(z)}{\hat{T}_L(z)} = \frac{H}{1 + \hat{H}_{FF}\hat{H}_{FB}H}\,. \tag{3.51}$$

A second relation is obtained from (3.50) and (3.51):

$$H_R(z) = \hat{H}_{FF}(z)\,H_L(z)\,. \tag{3.52}$$

The feedforward and feedback controllers can now be found from (3.49) and (3.52).

$$\hat{H}_{FF}(z) = H_L^{-1}(z)\,H_R(z)\,, \qquad \hat{H}_{FB}(z) = \hat{H}_{FF}^{-1}(z)\,\hat{G}(z)\,. \tag{3.53}$$

Recall the desired reference-to-output and disturbance-to-output transfer functions:

Reference: $$H_R(z) = \frac{0.307238\,z + 0.189566}{z^2 - 0.744495\,z + 0.241298}\,. \tag{3.54}$$

Disturbance: $$H_L(z) = \frac{z - 1}{z^2}\,. \tag{3.55}$$

Substitution of (3.54) and (3.55) into (3.53) obtains the controller transfer functions. The resulting two-degree-of-freedom wirefeed controller is given by

$$\hat{H}_{FF}(z) = \frac{0.307238\ z^3 + 0.189566\ z^2}{z^3 - 1.744495\ z^2 + 0.985793\ z - 0.241298} \quad . \tag{3.56}$$

$$\hat{H}_{FB}(z) = \frac{3.587452\ z^3 - 3.003382\ z^2 + 1.113222\ z - 0.080242}{z^3 + 0.617001\ z^2} \quad .$$

Plot 5 of Figure A.1 in the Appendix shows the magnitude of the disturbance-to-output transfer function for this wirefeed controller. Figure A.4 shows the results of a wirefeed experiment using the controller of (3.56). A comparison of the open-loop and the three controllers presented in this chapter is given in Figure A.5. The two-degree-of-freedom controller yields superior disturbance rejection at all frequencies.

CHAPTER 4.

ARC DYNAMICS MODEL

4.1. Overview of the Gas Metal Arc Welding Torch

The wire feed servo rotates a set of pinch rollers, which force the wire into the torch head and through the contact tube whereupon the wire is consumed by the welding process, as illustrated in Figure 4.1. The wire feed servo is in itself a feedback controlled system which is capable of delivering wire to the weld process at a controlled wire feed rate. For the purposes of this derivation, the wire feed rate $w_F(t)$ is considered to be the input. The arc dynamics form the *plant* and the arc current $i_a(t)$ is taken to be the output.

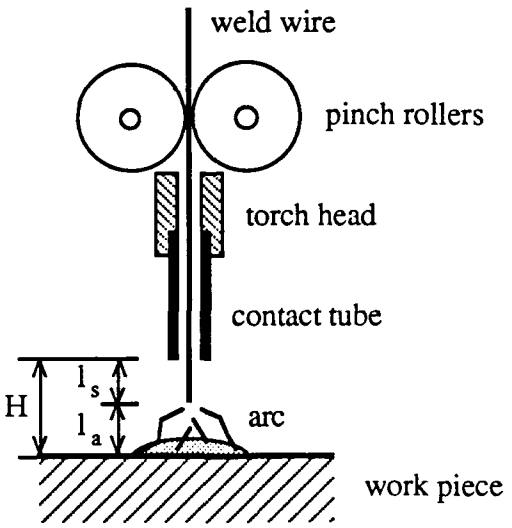

Figure 4.1. GMAW torch.

Assumption 4.1.

$$H = l_a(t) + l_s(t) = \textit{constant} \tag{4.1}$$

where H is the contact tube height, $l_a(t)$ is the arc length, and $l_s(t)$ is the stickout length. This assumption is motivated by careful examination of the side profile of the weld bead when the arc is abruptly extinguished. Figure 4.2 shows how the weld material piles up behind the arc as opposed to under it.

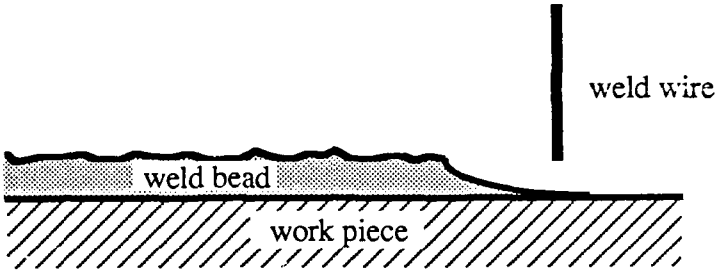

Figure 4.2. Side profile of weld bead.

Figure 4.3 shows the electrical model of the arc dynamics.

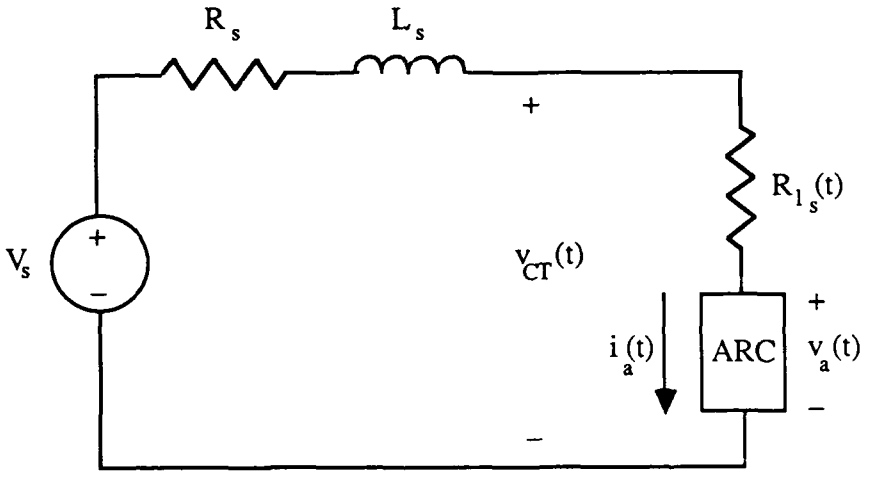

Figure 4.3. Electrical model.

Signals and Constants:

$v_a(t)$	arc voltage	V_s	open circuit voltage of arc welder power supply
$i_a(t)$	arc current	R_s	Thevenin resistance of arc welder power supply plus cabling resistance
$v_{CT}(t)$	contact tube voltage	L_s	inductance of arc welder power supply
		$R_{ls}(t)$	resistance of stickout length (time varying)

Assumption 4.2.

The electric arc is modeled as shown in Figure 4.4, where V_o is the sum of the cathode and anode voltage drops, E_o is the electric field intensity of the arc plasma, and $l_a(t)$ is the length of the electric arc.

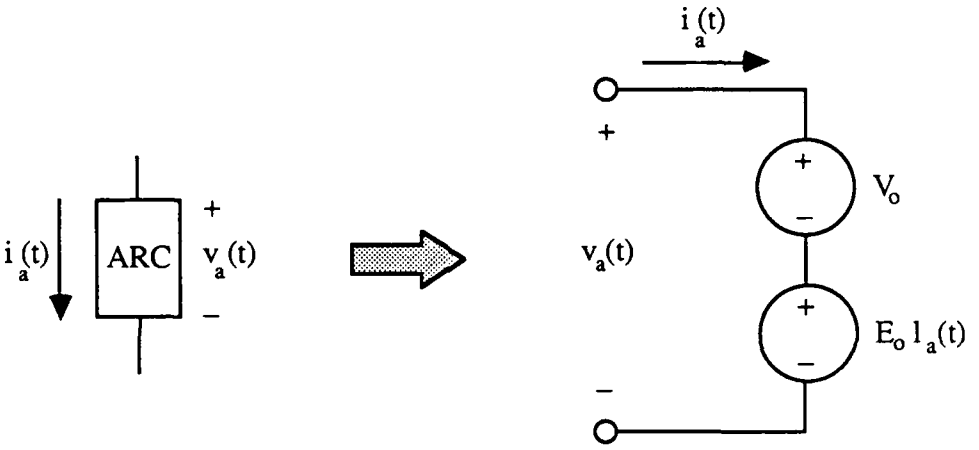

Figure 4.4. Arc model.

There are two modes associated with the arc:

τ_E = electrical mode; the arc can be modelled as a time varying conductance.

τ_T = thermodynamic mode; consumption of the wire.

Time constant τ_T exceeds τ_E by approximately two orders of magnitude. A static model is therefore used for the arc *electrical* circuit. However, the dynamics of wire consumption will not be ignored.

4.2. Development of the Dynamic Equations

Kirchhoff's Voltage Law applied to Figure 4.3 yields the electrical constraint equation,

$$V_s = R_s\, i_a(t) + L_s \frac{di_a(t)}{dt} + R_{ls}(t)\, i_a(t) + V_o + E_o\, l_a(t)\,. \tag{4.2}$$

The stickout length resistance $R_{ls}(t)$ can be written as a function of the arc length:

$$R_{ls}(t) = \frac{\rho}{A}\, l_s(t) = \frac{\rho}{A}\,[\, H - l_a(t)\,] \tag{4.3}$$

where ρ is the resistivity of the weld wire ($\Omega \cdot$ in) and A is the cross-sectional area of the weld wire. Substitution of (4.3) into (4.2) yields the electrical constraint equation in final form:

$$\frac{di_a(t)}{dt} = -\frac{1}{L_s}\left[\, R_s + \frac{\rho}{A} H \,\right] i_a(t) + \frac{\rho}{L_s A}\, i_a(t)\, l_a(t) - \frac{E_o}{L_s}\, l_a(t) + \frac{V_s - V_o}{L_s}\,. \tag{4.4}$$

Define $w_F(t)$ to be the feed rate of weld wire and define $w_C(t)$ to be the consumption rate of weld wire in inches per minute. Since $l_a(t)$ is the length of arc in inches, the following relation must hold:

$$\frac{dl_a(t)}{dt} = \frac{1 \text{ min}}{60 \text{ s}}\,[\, w_C(t) - w_F(t)\,]\,. \tag{4.5}$$

Following Waszink & Van Den Heuvel (1982),

$$w_C(t) = \frac{60 \text{ s}}{1 \text{ min}}\,[\, k_1\, i_a(t) + k_2\, i_a^2(t)\, l_s(t)\,]\,, \tag{4.6}$$

where the second term is due to joule heating.

Assumption 4.1 and Equations (4.5) and (4.6) yield the mechanical constraint equation:

$$\frac{dl_a(t)}{dt} = k_1\, i_a(t) + k_2\, H\, i_a^2(t) - k_2\, i_a^2(t)\, l_a(t) - \frac{1}{60}\,\omega_F(t)\,. \tag{4.7}$$

The arc current $i_a(t)$ and the contact tube voltage $v_{CT}(t)$ are measured quantities, while the arc length $l_a(t)$ is not measured. It is for this reason that an additional relation is of interest.

Kirchhoff's Voltage Law applied to an inner loop of Figure 4.3 gives

$$v_{CT}(t) = R_{ls}(t)\, i_a(t) + V_o + E_o\, l_a(t)\,. \tag{4.8}$$

Substitution of (4.3) into (4.8) allows $l_a(t)$ to be measured indirectly:

$$v_{CT}(t) = \frac{\rho\, H}{A} i_a(t) - \frac{\rho}{A} i_a(t)\, l_a(t) + E_o\, l_a(t) + V_o\,. \tag{4.9}$$

Summary of the arc dynamics model:

$$\frac{di_a(t)}{dt} = -\frac{1}{L_s}\left[R_s + \frac{\rho}{A} H \right] i_a(t) + \frac{\rho}{L_s A} i_a(t)\, l_a(t) - \frac{E_o}{L_s} l_a(t) + \frac{V_s - V_o}{L_s}$$

$$\frac{dl_a(t)}{dt} = k_1\, i_a(t) + k_2\, H\, i_a^2(t) - k_2\, i_a^2(t)\, l_a(t) - \frac{1}{60} w_F(t) \tag{4.10}$$

$$v_{CT}(t) = \frac{\rho\, H}{A} i_a(t) - \frac{\rho}{A} i_a(t)\, l_a(t) + E_o\, l_a(t) + V_o$$

where

$i_a(t)$ = arc current,

$l_a(t)$ = arc length,

$v_{CT}(t)$ = contact tube voltage,

$w_F(t)$ = wire feed rate,

V_S = open circuit voltage of power supply,

R_S = resistance of power supply and cabling,

L_S = inductance of power supply,

ρ = resistivity of weld wire,

A = cross-sectional area of weld wire,

H = contact tube height,

V_o = sum of cathode and anode voltage drops,

E_o = electric field intensity of arc plasma,

k_1, k_2 = wire consumption rate constants.

4.3. Calculation of the Parameter Values

The following nominal operating point (measured experimentally) is used as a basis:

i_a = 340 A. v_{CT} = 31 V.

l_a = 0.25 in. ω_F = 300 IPM.

The power supply is set for a V_S of 40 V, and the manufacturer's specifications show an L_S of 400 μH. The 0.0625-inch diameter weld wire has a cross-sectional area A of 3.068×10^{-3} in^2. The contact tube height H is set at 1 in. Wu & Richardson (1984) approximate ρ at 40 μΩ·in. Table A.1 of that paper yields an E_o of 26 $V \cdot in^{-1}$.

For the calculation of V_o and R_S, consider the electrical model in steady-state as shown in Figure 4.5.

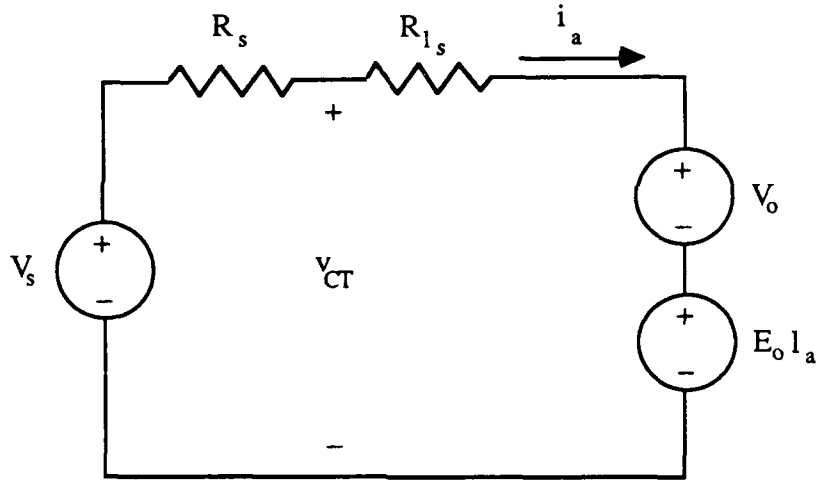

Figure 4.5. Electrical model in steady-state.

Analysis of the circuit in steady-state yields the following relations:

$$R_S = \frac{V_S - v_{CT}}{i_a},$$

$$V_o = V_{CT} - E_o l_a - R_{ls} i_a = V_{CT} - E_o l_a - \frac{\rho}{A}(H - l_a) i_a . \qquad (4.11)$$

Substitution of the numerical values gives an R_S of 0.02647 Ω and a V_o of 21.18 V.

Estimation of the constants k_1 and k_2 requires use of experimental data. Curve fitting with actual welding runs yielded the approximate relation

$$w_C = 0.59398\, i_a + 0.00047164\, i_a^2 , \tag{4.12}$$

where w_C is in inches per minute and i_a is in Amps. Setting (4.12) equal to (4.6) gives

$$0.59398\, i_a + 0.00047164\, i_a^2 = 60\,(k_1\, i_a + k_2\, i_a^2\, l_s) . \tag{4.13}$$

Substitution of the operating point values for i_a and l_s into (4.13) gives

$$k_1 = 9.8997\text{x}10^{-3}\ \text{in}\cdot\text{A}^{-1}\cdot\text{s}^{-1} , \qquad k_2 = 1.0481\text{x}10^{-5}\ \text{A}^{-2}\cdot\text{s}^{-1} .$$

These values of k_1 and k_2 yield a wire consumption rate w_C of 260 IPM for an arc current of 340 A. This rate is within 10% of the experimentally measured operating point value.

The arc dynamics model is now complete with numerical coefficients.

Arc dynamics model:

$$\frac{di_a(t)}{dt} = -9.8770\text{x}10^{1}\, i_a(t) + 3.2595\text{x}10^{1}\, i_a(t)\, l_a(t) - 6.5\text{x}10^{4}\, l_a(t) + 4.705\text{x}10^{4}$$

$$\frac{dl_a(t)}{dt} = 9.8997\text{x}10^{-3}\, i_a(t) + 1.0481\text{x}10^{-5}\, i_a^2(t) - 1.0481\text{x}10^{-5}\, i_a^2(t)\, l_a(t) - 1.667\text{x}10^{-2}\, w_F(t) \tag{4.14}$$

$$v_{CT}(t) = 1.3038\text{x}10^{-2}\, i_a(t) - 1.3038\text{x}10^{-2}\, i_a(t)\, l_a(t) + 2.50\text{x}10^{1}\, l_a(t) + 2.118\text{x}10^{1}$$

with $i_a(t)$ in amperes, $l_a(t)$ in inches, $v_{CT}(t)$ in volts, and $w_F(t)$ in inches per minute.

4.4. Linearization of the Model

A linear approximation to the arc dynamics model is used for the controller design. Define input u(t) to be the wire feed rate $w_F(t)$. Define state $x_1(t)$ to be the arc current $i_a(t)$, and define state $x_2(t)$ to be the arc length $l_a(t)$ in order to write the nonlinear state equations of (4.15).

$$\dot{x}_1(t) = c_1 x_1(t) + c_2 x_1(t) x_2(t) + c_3 x_2(t) + d_1 \quad := f_1(x_1, x_2) + d_1$$
$$\dot{x}_2(t) = c_4 x_1(t) + c_5 x_1^2(t) + c_6 x_1^2(t) x_2(t) + b_2 u(t) := f_2(x_1, x_2) + b_2 u \qquad (4.15)$$

Now, make some further definitions:

$$x := \begin{bmatrix} x_1 \\ x_2 \end{bmatrix}, \quad f(x) := \begin{bmatrix} f_1(x_1, x_2) \\ f_2(x_1, x_2) \end{bmatrix}, \quad b := \begin{bmatrix} 0 \\ b_2 \end{bmatrix}, \quad d := \begin{bmatrix} d_1 \\ 0 \end{bmatrix}; \qquad (4.16)$$

$$a_{ij} := \frac{\partial f_i(x_1, x_2)}{\partial x_j}, \qquad A := \begin{bmatrix} a_{11} & a_{12} \\ a_{21} & a_{22} \end{bmatrix}. \qquad (4.17)$$

Using the above vector notation, the system becomes

$$\dot{x} = f(x) + bu + d. \qquad (4.18)$$

Furthermore, the linearized system is given by

$$\delta\dot{x} = A\,\delta x + b\,\delta u, \qquad (4.19)$$

where the partial derivatives of the A matrix are evaluated at a *nominal operating point* x_{nom} and the variables δx and δu represent reasonably small *perturbations* from this operating point (Brogan (1982)). The partial derivatives of (4.15) are taken to obtain

$$a_{11} = c_1 + c_2 x_2, \qquad a_{12} = c_2 x_1 + c_3,$$
$$a_{21} = c_4 + 2 c_5 x_1 + 2 c_6 x_1 x_2, \qquad a_{22} = c_6 x_1^2. \qquad (4.20)$$

Now, since the arc current $i_a(t)$ is the variable to be regulated and the arc length $l_a(t)$ is not really of interest, define the system output y(t) to be the arc current state variable $x_1(t)$. In vector notation,

$$\delta y = c\,\delta x; \qquad c := [\,1 \;\; 0\,]. \qquad (4.21)$$

Finally, the single-input, single-output system of (4.19) and (4.21) has a transfer function H(s) that is given by

$$H(s) = c(sI - A)^{-1} b. \qquad (4.22)$$

If the characteristic polynomial of A is denoted by $\Delta(s)$, then H(s) can be written as

$$H(s) = \frac{a_{12}\, b_2}{\Delta(s)} ; \qquad \Delta(s) = s^2 - (a_{11} + a_{22})\, s + (a_{11}\, a_{22} - a_{12}\, a_{21}) . \tag{4.23}$$

Consider three values for the arc current; 200 A, 340 A, and 400 A. These values span the range of reasonable arc currents for welding. Now consider the nonlinear dynamic equations of (4.14) in *steady-state* (derivatives equal to zero). These equations can be used to find steady-state values for the arc length and the wire feed rate that correspond to each arc current.

$$\begin{aligned} 0 &= -9.8770\text{x}10^{1}\, i_a + 3.2595\text{x}10^{1}\, i_a\, l_a - 6.5\text{x}10^{4}\, l_a + 4.705\text{x}10^{4} \\ 0 &= 9.8977\text{x}10^{-3}\, i_a + 1.0481\text{x}10^{-5}\, i_a^2 - 1.0481\text{x}10^{-5}\, i_a^2\, l_a - 1.667\text{x}10^{-2}\, w_F \end{aligned} \tag{4.24}$$

Substitution of the arc currents into (4.24) yields the following three operating points:

$$\begin{aligned} i_a &= 200 \text{ A.} \quad \Rightarrow \quad l_a = 0.4668 \text{ in}, \quad w_F = 132 \text{ IPM}, \\ i_a &= 340 \text{ A.} \quad \Rightarrow \quad l_a = 0..2498 \text{ in}, \quad w_F = 256 \text{ IPM}, \\ i_a &= 400 \text{ A.} \quad \Rightarrow \quad l_a = 0.1451 \text{ in}, \quad w_F = 324 \text{ IPM}. \end{aligned} \tag{4.25}$$

Substitution of the numerical values of (4.14) and (4.25) into the relations of (4.15), (4.20), and (4.23) yields the following three linearized arc dynamics transfer functions:

$$H(s)_{200A} = \frac{974.68}{s^2 + 83.975\, s + 744.72} , \tag{4.26}$$

$$H(s)_{340A} = \frac{898.63}{s^2 + 91.839\, s + 931.86} , \tag{4.27}$$

$$H(s)_{400A} = \frac{866.04}{s^2 + 95.700\, s + 1044.6} . \tag{4.28}$$

Figure 4.6 shows how the poles of the linearized transfer function H(s) vary (in rad/sec) with respect to nominal arc current. This variation is smooth and moderate, suggesting that a single H(s) can be used for the design of the arc current controller. Choose this nominal transfer function to be the 340 A H(s) of equation (4.27).

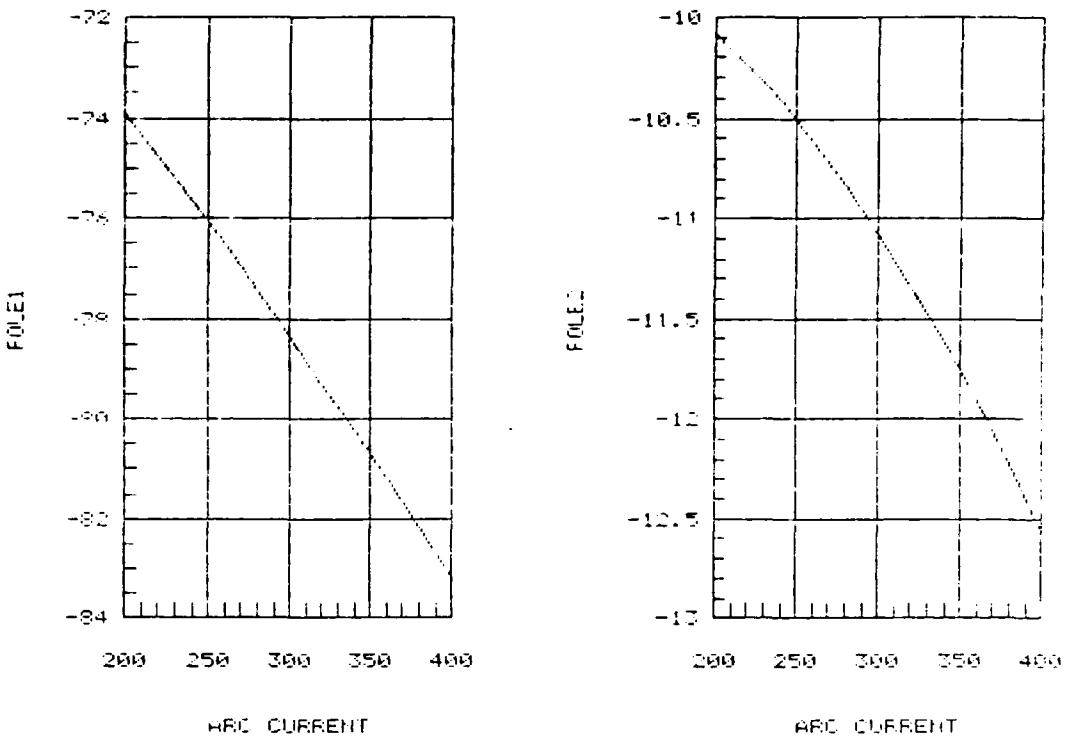

Figure 4.6. Pole locations versus nominal arc current.

CHAPTER 5.

ARC CURRENT CONTROLLER DESIGN

Chapter 4 ended with the development of a nominal continuous-time transfer function that relates arc current to wire feed rate. Although the arc dynamics are nonlinear, it was shown that the poles of the linearized system do not shift radically when the nominal operating point is varied. It is therefore reasonable to use this nominal transfer function for the arc current controller design.

Chapter 2 posed the reference-tracking objectives for the wire feed servo in terms of a desired reference-to-output transfer function. This transfer function was matched by the controller that was designed in Chapter 3.

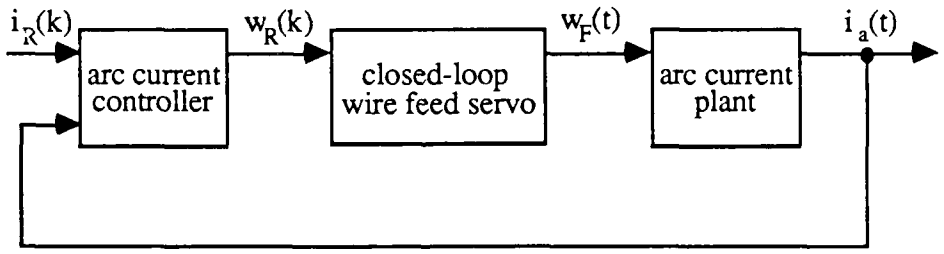

Figure 5.1. Closed-loop arc current system.

Figure 5.1 shows the arc current system with $i_a(t)$ and $i_R(k)$ given in amperes, and $w_F(t)$ and $w_R(k)$ given in inches per minute. The closed-loop system is required to have a bandwidth of 1 Hz. Furthermore, the closed-loop step response should be without overshoot. The system is to be mildly overdamped. Zero steady-state tracking error is required for constant reference inputs. The arc current controller will be designed in a continuous-time setting and then discretized for computer implementation.

The design objectives are not difficult but the plant is nonlinear with uncertain parameters. For this reason, a simple and robust proportional-integral controller will be used for the design. Robust stability of the arc current is of primary importance for reasons of safety as well as weld quality.

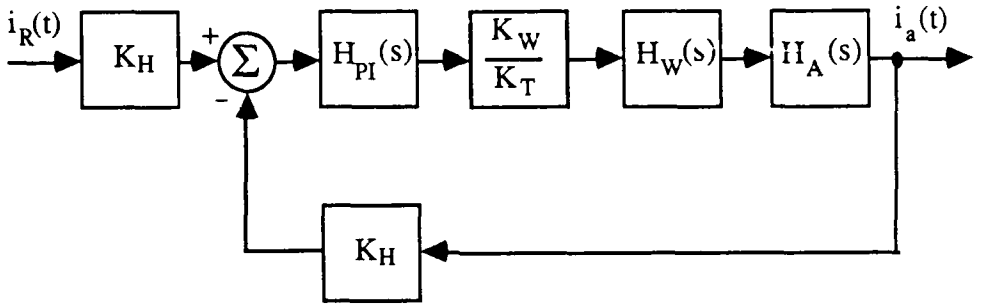

Figure 5.2. Continuous-time arc current block diagram.

Figure 5.2 shows the arc current system in a continuous-time format. The output $i_a(t)$ of the arc current plant and the reference input $i_R(t)$ are given in amperes. A "Hall effect" sensor produces a voltage that is proportional to the arc current. A constant K_H of 1 V per 100 A models this sensor. The constant K_W/K_T converts volts to inches per minute. Its value is found in Chapter 2 to be 194.95 IPM per volt. Finally, the wire feed servo has its input and output given in inches per minute.

Chapters 2 and 4 give the closed-loop wire feed servo and the open-loop arc current transfer functions.

$$\text{Closed-loop wire feed:} \qquad H_W(s) = \frac{631.655}{s^2 + 35.5431s + 631.655} . \tag{5.1}$$

$$\text{Open-loop arc current:} \qquad H_A(s) = \frac{898.631}{s^2 + 91.8393s + 931.862} . \tag{5.2}$$

The proportional-integral arc current controller is of the form

$$H_{PI}(s) = K_P + \frac{K_I}{s} = \frac{K_P s + K_I}{s} . \tag{5.3}$$

The controller design is simplified by introducing the *normalized* model of Figure 5.3.

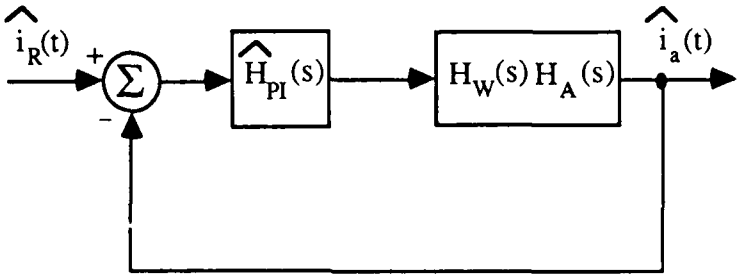

Figure 5.3. Normalized arc current system.

where

$$\hat{i}_R(t) = K_H\, i_R(t)\,, \qquad \hat{i}_a(t) = K_H\, i_a(t)\,,$$

and

$$\hat{H}_{PI}(s) = \hat{K}_P + \frac{\hat{K}_I}{s} = \frac{K_W\, K_H}{K_T}\, H_{PI}(s)\,. \tag{5.4}$$

The composite plant $H_W(s)H_A(s)$ is fourth order with relative degree four. To this we append a first-order controller, creating a fifth-order closed-loop system. A purely analytic design of $\hat{H}_{PI}(s)$ to achieve a desired closed-loop bandwidth and damping would be difficult. For this reason, the design was accomplished with the aid of iterative computer simulation. Integrator gain was adjusted to achieve the desired bandwidth, and then the proportional gain was tuned to create a mildly overdamped step response. The resulting gains are

$$\hat{K}_P = 0.29\,, \qquad \hat{K}_I = 4.20\,. \tag{5.5}$$

Thus the continuous-time proportional-integral controller is given by

$$\hat{H}_{PI}(s) = 0.29 + \frac{4.20}{s}\,. \tag{5.6}$$

A simple Euler approximation with a sampling period T_S of 0.04 second is used for the discretization of the PI controller. The resulting *proportional-sum* controller is

$$\hat{H}_{PS}(z) = \hat{K}_P + \frac{\hat{K}_I T_S}{z - 1} = 0.29 + \frac{0.168}{z - 1} = \frac{0.29z - 0.122}{z - 1} . \qquad (5.7)$$

Figure A.6 of the Appendix shows an experimental welding run. The arc current controller was stepped across nearly the entire operating range to show the robust quality of the design. The upper plot shows the arc current and the lower plot shows the closed-loop wirefeed reference $w_R(t)$ (dashed line) and the wirefeed servo output $w_F(t)$ (solid line).

CHAPTER 6.

CONCLUSIONS

From an academic point of view, the work exhibits some diversity. In Chapter 2 a wire feed plant is developed which has simple linear dynamics but is corrupted by a severe torque disturbance. This model is discretized and Chapter 3 presents three discrete-time controller designs which vary considerably in performance, complexity, and design philosophy. Chapter 4 develops a nonlinear arc dynamics model which is linearized for the controller design. Finally, in Chapter 5 a continuous-time arc current controller is designed and then discretized for computer implementation.

The plots in the Appendix give testimony to the success of the final design. The torque disturbance in the wire feed servo has been virtually eliminated while the servo exhibits desirable reference-to-output characteristics. The fixed-parameter arc current controller is well behaved at all operating points and is capable of stepping the arc current the full 100 A of its useful range.

APPENDIX

SELECTED PLOTS

This appendix presents experimental data as well as computer simulated results. These plots are gathered together to facilitate a convenient performance comparison of the various controller designs. All Fourier transforms are presented on a decibel scale and have been normalized by dividing by the average value of the time domain signal.

Figure A.1 gives various magnitude plots that pertain to the wire feed servo controller design. In numbered order these plots are: the open-loop plant, the desired reference-to-output transfer function, and the closed-loop disturbance-to-output for the proportional-sum, polynomial, and two-degree-of-freedom controller designs.

Figure A.2 shows open-loop experimental data. Time domain plots and resulting Fourier transforms are given for the wire feed rate and for the resulting arc current. Figures A.3 through A.5 show experimental results for the three wire feed servo controller designs. Figure A.6 shows experimental step response data for the final closed-loop arc current controller.

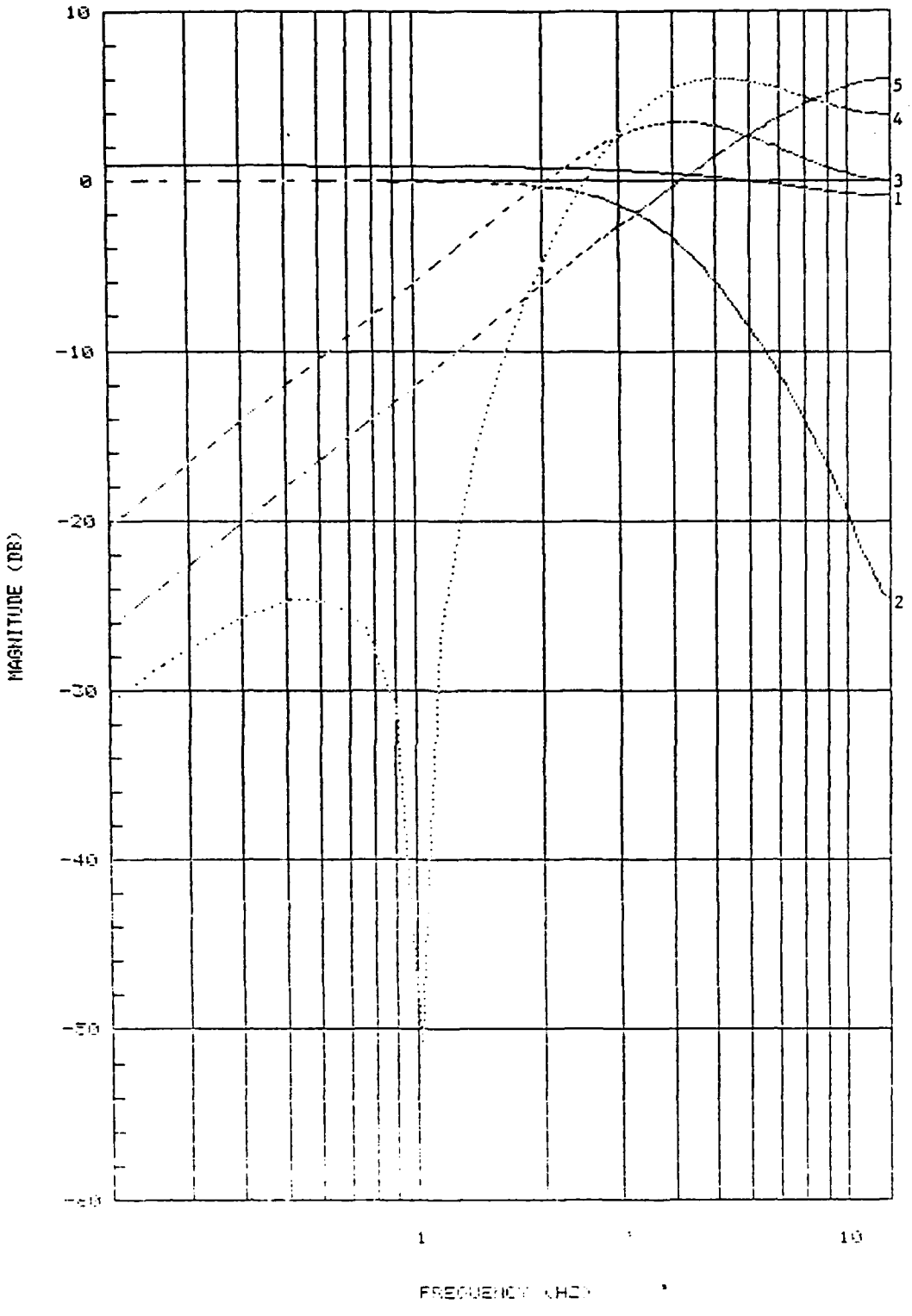

Figure A.1. Magnitude plots for wire feed servo.

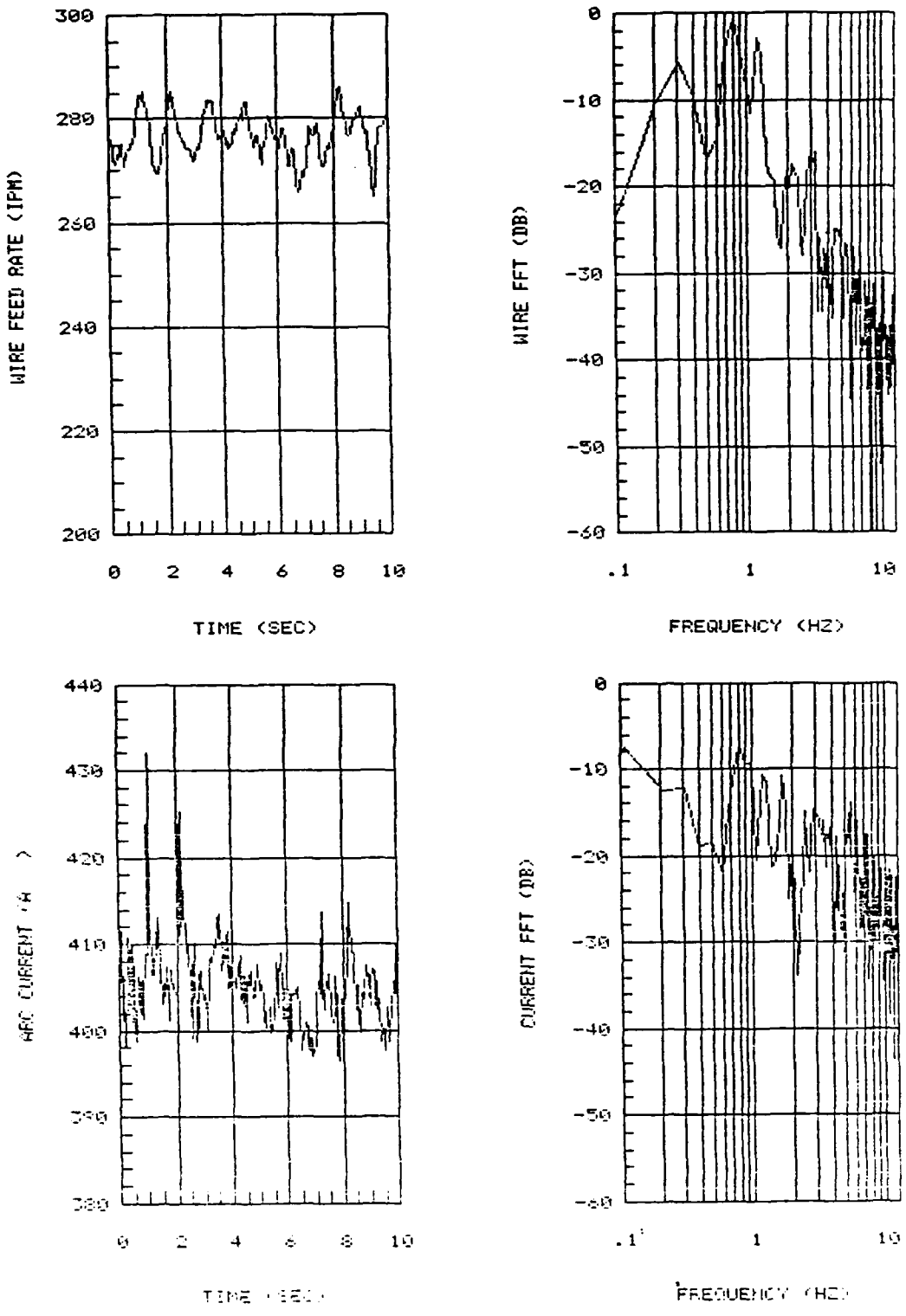

Figure A.2. Open-loop experimental data.

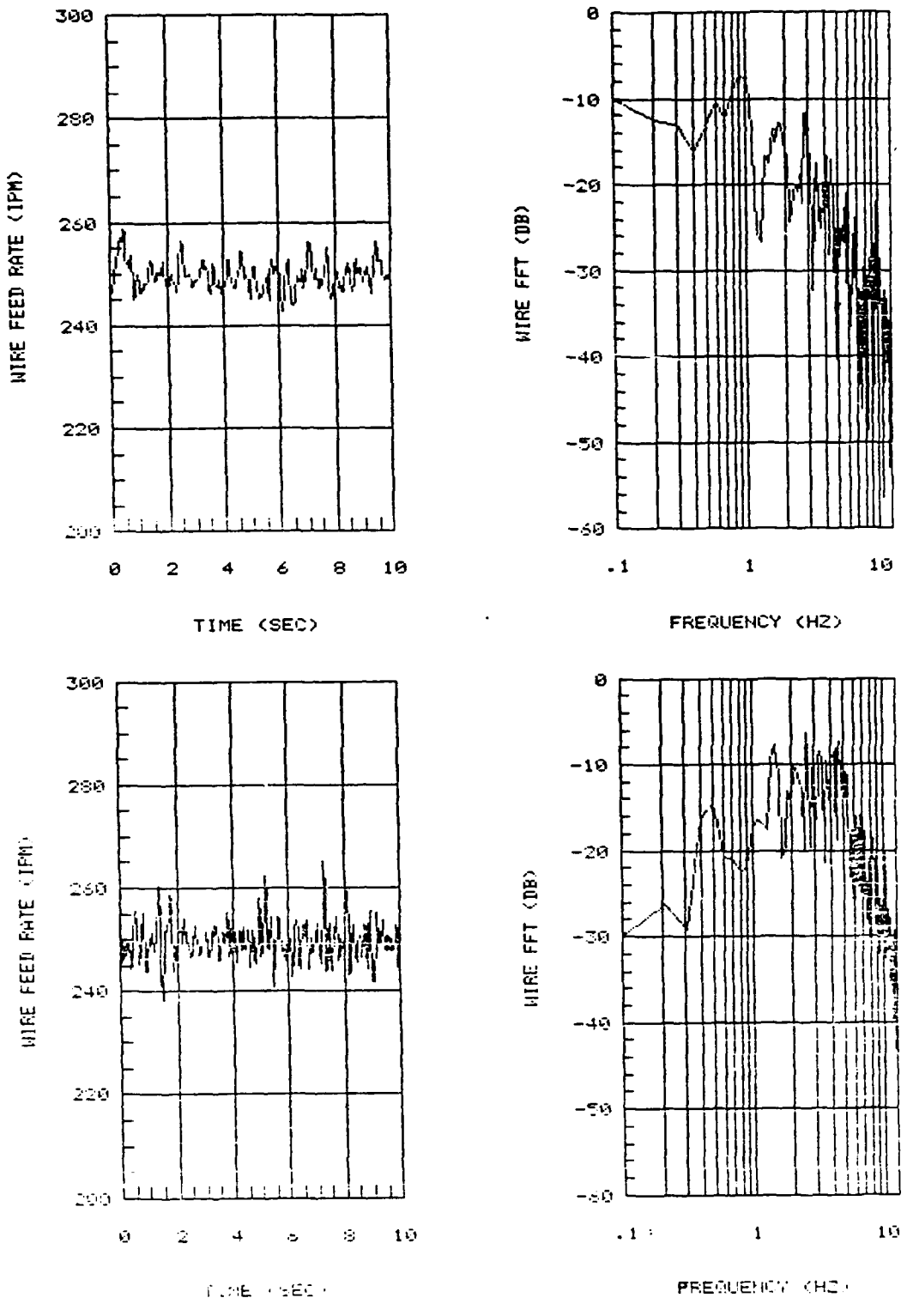

Figure A.3. Wirefeed servo experimental data: PS control (top) and polynomial method (bottom).

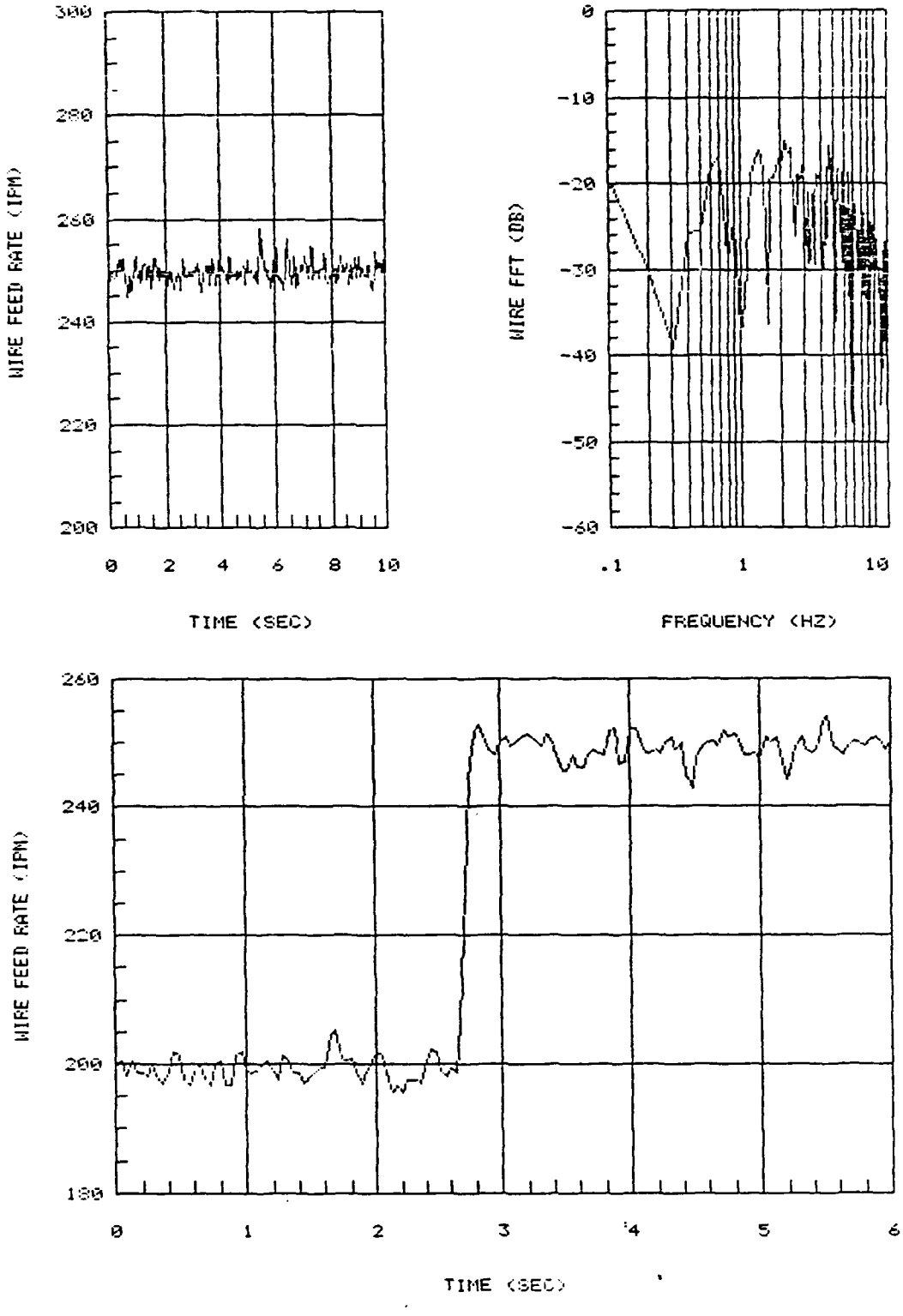

Figure A.4. Wirefeed servo experimental data: Two-degree-of-freedom controller.

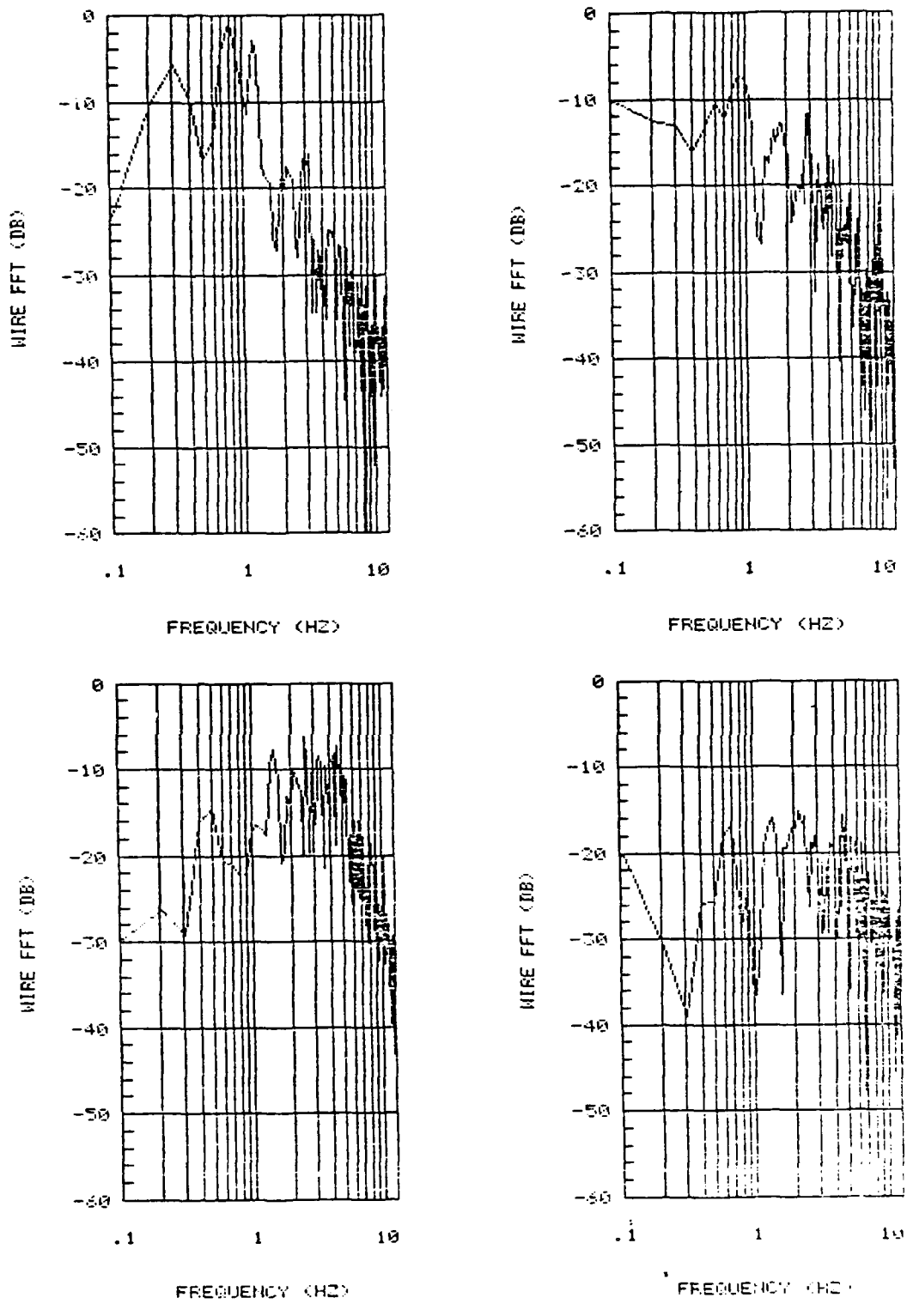

Figure A.5. Open-loop, PS, polynomial, and TDF wirefeed FFT comparison.

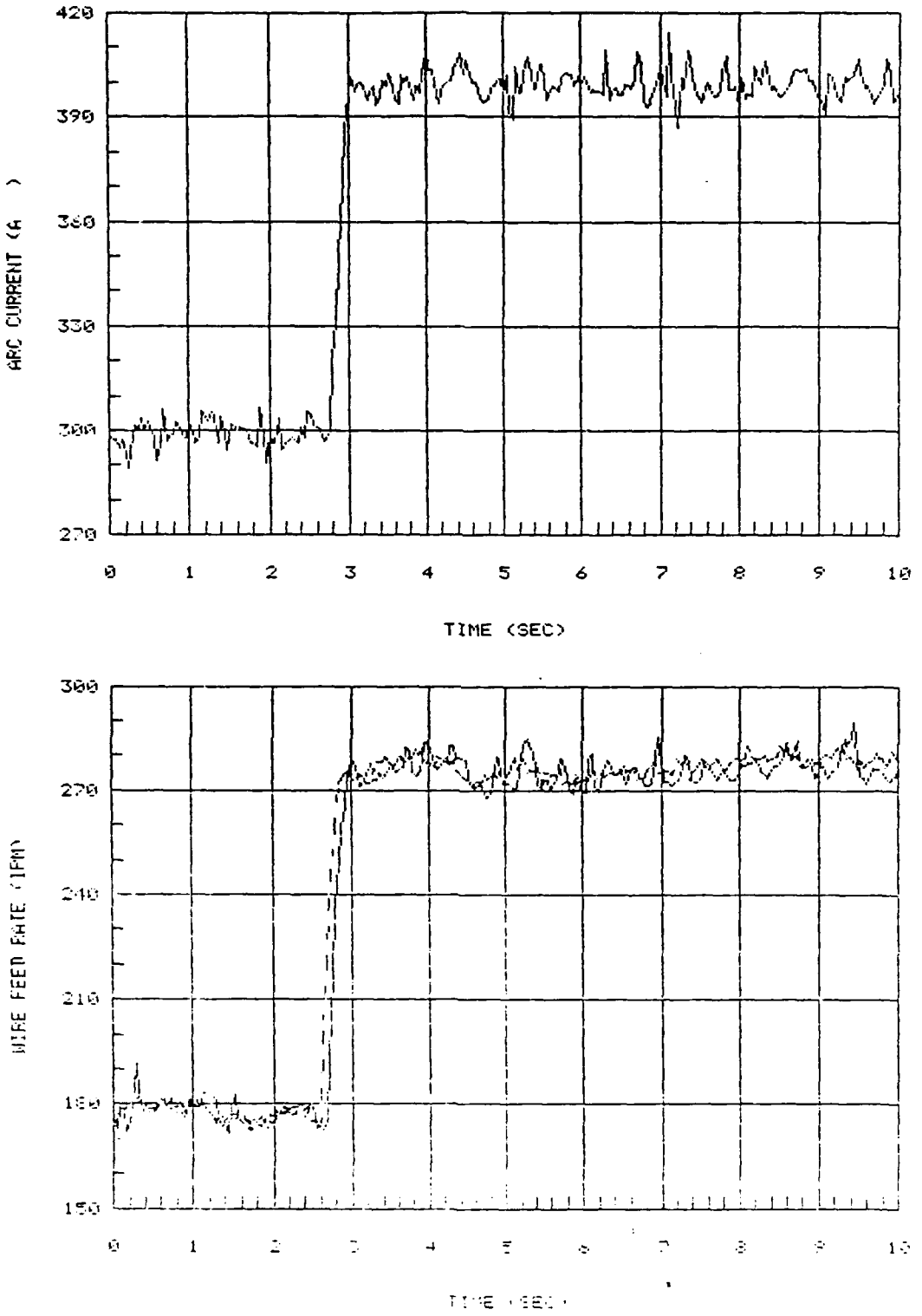

Figure A.6. Closed-loop arc current controller experimental step response data.

REFERENCES

Astrom, K. J. and B. Wittenmark, 1984, *Computer Controlled Systems Theory and Design,* Engelwood Cliffs: Prentice Hall.

Brogan, W. L., 1982, *Modern Control Theory,* Engelwood Cliffs: Prentice-Hall.

Franklin, G. F. and J. D. Powell, 1980, *Digital Control of Dynamic Systems,* Reading: Addison-Wesley Publishing Company.

Kuo, B. C., 1980, *Digital Control Systems,* New York: Holt, Rinehart and Winston.

Waszink, J. H. and G. J. Van Den Heuvel, 1982, "Heat Generation and Heat Flow in the Filler Metal in GMA Welding," *Welding Journal Research Suppliment,* Vol. 61-8.

Wu, G. D. and R. W. Richardson, 1984, "The Dynamic Response of Self-Regulation of the Welding Arc," *GWR Technical Report,* No. 529501-84-23.